ELSEVIER

Journal of Volcanology and Geothermal Research 116 (2002) 35–61

Journal of volcanology and geothermal research

www.elsevier.com/locate/jvolgeores

The mineralogy of the Kokchetav 'lamproite': implications for the magma evolution

Yongfeng Zhu [a,b,*], Yoshihide Ogasawara [b], T. Ayabe [b]

[a] *Department of Geology, Peking University, Beijing 100871, PR China*
[b] *Department of Earth Sciences, Waseda University, Tokyo 169-8050, Japan*

Received 4 December 2001; received in revised form 4 December 2001; accepted 4 December 2001

Abstract

Kokchetav 'lamproite' occurs in the east end of Kokchetav massif and consists of phenocryst (mainly clinopyroxene) and matrix (mainly feldspar). The compositions of clinopyroxene, magnetite and biotite phenocryst were determined using wavelength dispersive spectrometry on a JEOL Super-probe 8900 electron microprobe for the purpose of revealing the process of magma evolution. Analyses revealed a core–rim variation, which is consistent with three stages of magmatic evolution: Mg-rich clinopyroxene cores (diopside) and biotite cores (phlogopite) crystallized in a deep magma chamber (stage I); Fe-rich clinopyroxene rim (salite) and biotite rim crystallized at low pressure in a shallow magma chamber (stage II); Magnetite phenocryst core also crystallized in a shallow magma chamber, and co-exists with Fe-rich clinopyroxene rim and biotite rim. The magnetite rims probably formed during magma eruption at the same time when groundmass crystallized (stage III). The calculated temperatures for ilmenite–magnetite pair range from 679 to 887°C, log fO_2 values range from −11.1 to −14.9 log units. These values represent the latest conditions of magma as ilmenite exsolution in magnetite probably occurred during magma eruption from the shallow chamber to surface.

Keywords: clinopyroxene; magnetite; mantle petrology; lamproite; Kokchetav

1. Introduction

Lamproites are ultrapotassic igneous rocks and are known on all continents. Despite their small volumes and petrologic peculiarities, lamproites can potentially provide much intrinsic information on the nature and evolution of their mantle source regions. In addition study of their genesis provides some interesting tectonic insights into the nature of postrift and postcollisional mantle lithospheric magmatism (Mitchell and Bergman, 1991). Lamproitic rocks therefore were intensively studied all over the world. Recently, a new lamproite locality was found in the Kokchetav massif, north Kazakhstan.

Kokchetav massif consists of diamond-bearing ultrahigh pressure (UHP) and high pressure (HP) units, and extends about 80 km along NW–SE with a width of around 17 km (Dobretsov et al., 1995). The Kokchetav UHP and HP metamorphic belts are composed of Precambrian protoliths that are overlain by the Cambro-Ordovician volcanic

* Corresponding author. Fax: 81-3-3207-495.
E-mail address: yongfeng@eyou.com (Y. Zhu).

0377-0273/02/$ – see front matter
PII: S0377-0273(01)00335-3

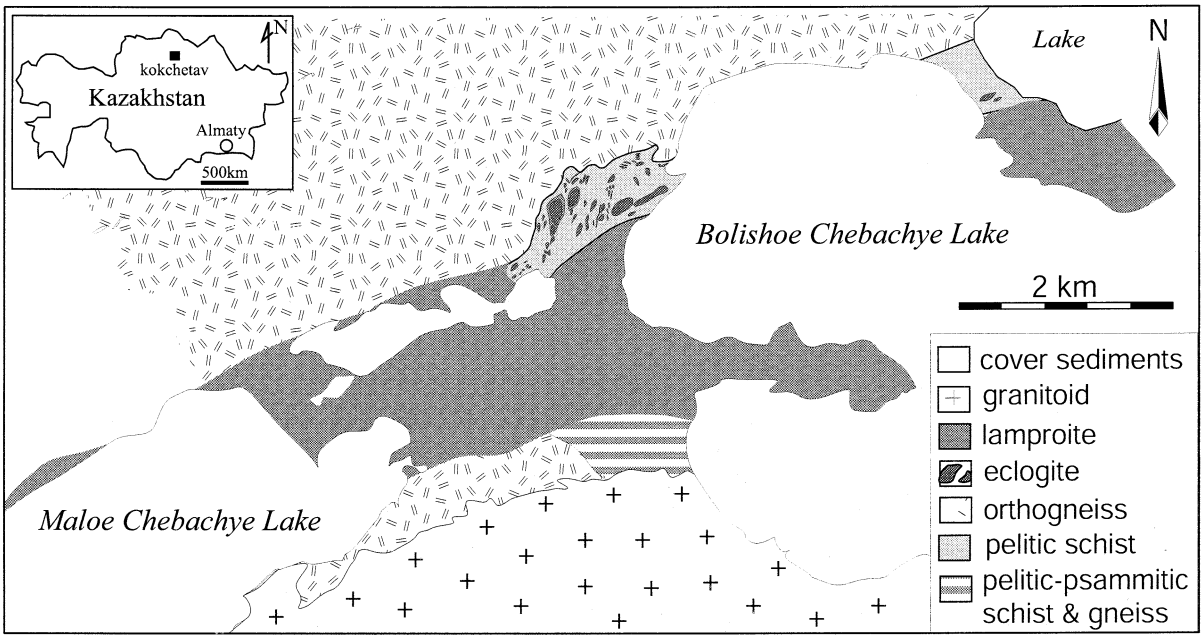

Fig. 1. Geological map of the Kokchetav 'lamproite' (modified from Kaneko et al., 2000).

and sedimentary strata of mainly island arc origin, Devonian volcanic molasses, and Carboniferous and Triassic shallow water and lacustrine deposits (Kaneko et al., 2000). Silurian to Early Devonian syn-tectonic granites and Late Devonian to Carboniferous postcollisional granitoids intruded into the metamorphic belts (Dobretsov et al., 1995). Metamorphism of the diamond-bearing parageneses, schists and associated tectonic rocks took place in the Middle Cambrian, as indicated by Sm–Nd and U–Pb ages between 520 and 540 Ma (Jagoutz et al., 1990; Claoue-Long et al., 1991; Shatsky et al., 1999). These authors suggest that the collision of micro-continents during the Lower Paleozoic resulted in the sinking of thinned crust to a depth of about 150 km.

Although the UHP metamorphism and tectonic evolution of Kokchetav massif have been extensively studied, the postcollisional processes of this massif and the characteristics of its lithospheric mantle are poorly understood. Kokchetav 'lamproite' occurs in Kokchetav massif as a postcollisional magmatic phase (Kaneko et al., 2000) and provides a chance to study the nature of its mantle source after UHP metamorphism. This manuscript reports the compositions of major mineral phases of Kokchetav 'lamproite' for the purpose of revealing the processes of magma evolution.

2. Geological setting and petrography

Kokchetav 'lamproites' occur in the Boroboye uplift area as tuff breccia, at the east end of Kokchetav massif, on the north banks of Maloe Chebachye Lake and Bolishoe Chebachye Lake (Fig. 1). In the north, country rocks are UHP rocks including diamond-bearing acidic gneiss and ecologite-bearing pelitic schist. The country rocks in southern parts are pelitic psammitic schist and gneiss, which were intruded by Devonian granitoids. The contact boundaries between the 'lamproites' and the country rocks are faults. Lamproites extend more than 13 km in NE-E direction, and are covered by lake-deposits and water (Fig. 1). The outcrop area is about 10 km^2.

The Kokchetav 'lamproite' is rather fresh with a low degree of alteration, which mainly occurs in

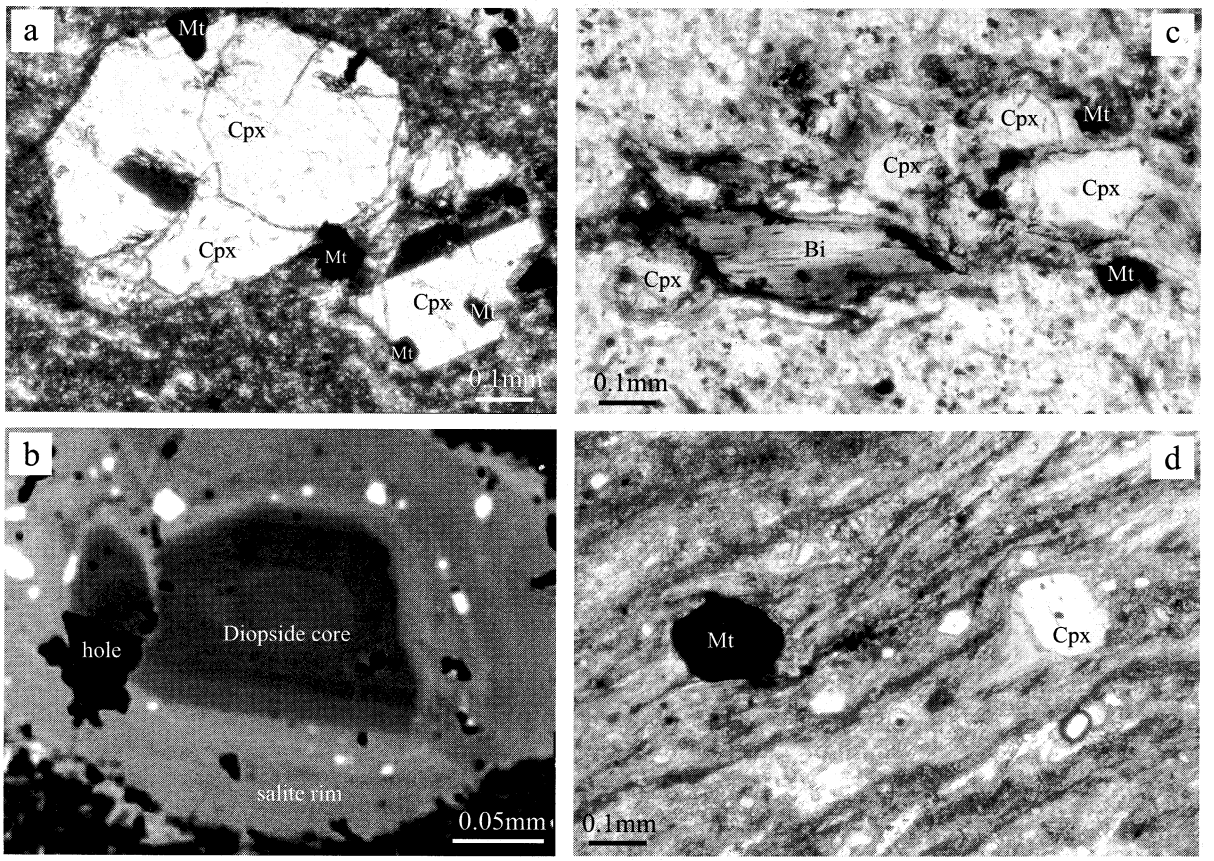

Fig. 2. (a) Clinopyroxene (Cpx) phenocryst with magnetite (Mt). The clinopyroxene shows broken and resorbed outlines. Cross-polarized light. (b) Back-scattered electron image of a zoned clinopyroxene with diopside core and salite rim. There are abundant magnetite inclusions (light) in clinopyroxene rim; (c) one biotite (Bi) and several clinopyroxene phenocrysts (+magnetite) are replaced by actinolite along their rims. All clinopyroxene crystals show irregular shapes (resorbed and broken). Single polarized light. (d) Clinopyroxene and magnetite phenocryst in the matrix with rhyotaxitic texture. Single polarized light.

the groundmass and the rims of the phenocrysts. The rock is porphyritic, with 30–50 vol.% phenocrysts, mostly clinopyroxene. Clinopyroxene typically forms colorless micro-phenocryst (mainly 0.1–0.6 mm and rarely up to 1.5 mm in length), some of them are simply twinned. The clinopyroxene in many instances is partially dissolved and has, evidently, undergone resorption in rims (Fig. 2a). Clinopyroxene is zoned with diopside core and salite rim. Ti–magnetite occurs in the clinopyroxene rim (Fig. 2b). This is quite different from most lamproites, as pyroxenes in lamproite are typically not zoned. Rare exceptions to this rule occur in rocks from the Leucite Hills, which are zoned to Fe-rich rims and exhibit acmitic mantles (Mitchell, 1995). In rare case, biotite occurs as a phenocryst phase co-existing with clinopyroxene and magnetite. Actinolite replaces clinopyroxene and biotite rims in some cases (Fig. 2c). The rhyotaxitic texture is developed in some cases for matrix (Fig. 2d). The groundmass consists mainly of feldspar with trace amounts of apatite and magnetite. Feldspar is replaced by epidote and fabric actinolite partially. Magnetite occurs both as phenocryst and matrix, and magnetite grain can be as large as clinopyroxene phenocryst (Fig. 2d). Magnetite phenocryst has a complex structure. Its core contains abundant blebby il-

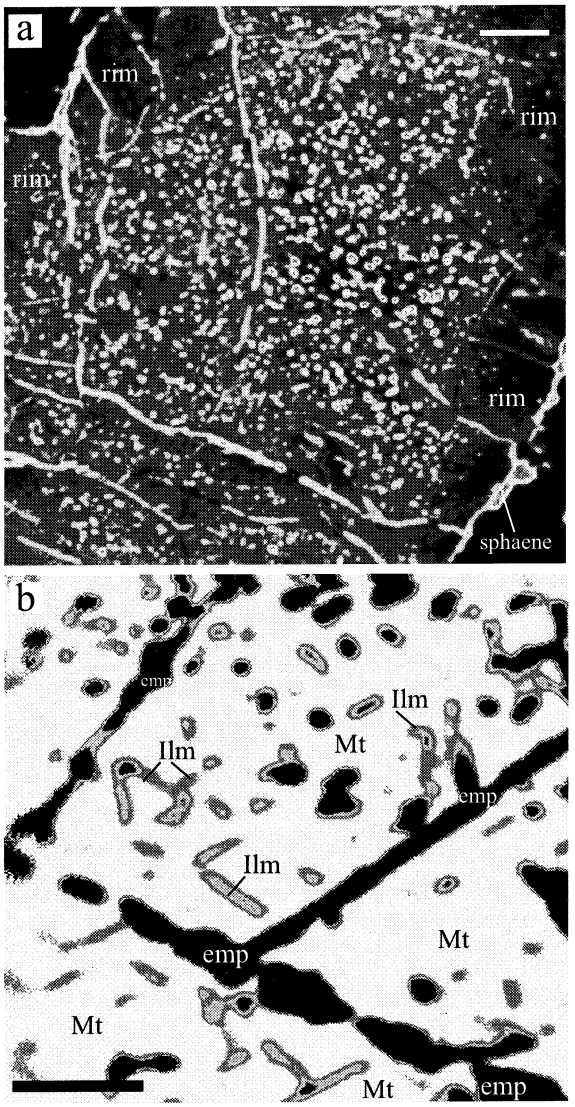

Fig. 3. (a) The X-ray image (Ti) of a magnetite phenocryst. Noting abundant ilmenite inclusions in magnetite core and inclusion-free rim. The cracks are filled with sphene veins cutting through magnetite and marking magnetite outlines. The scale bar is 20μ m. (b) The X-ray image (Fe) of the local area of magnetite core, where ilmenite (Ilm) arranges in two directions, which is parallel with some empty (emp). The scale bar is 5 μm.

menite inclusions but its rim is inclusion-free (Fig. 3a). Magnetite phenocryst generally is marked by a thin (about 1 μm in width, discontinuous) sphene band. The sphene band connects to ilmenite inclusions in magnetite core along cracks cutting through the magnetite rim (Fig. 3a). The tiny ilmenite inclusions (between 0.1×0.1 and 0.1×3 μm in size) in the magnetite core should be the products of exsolution as they arranged exactly in two orientations as shown in Fig. 3b. Some cracks are parallel to the orientation of the exsolved ilmenite as shown in Fig. 3a,b. Others, however, have different orientation, which cut across the orientation of the exsolution (see Fig. 3a). Most cracks are filled with sphene (Fig. 3a), but others are empty, showing the shapes similar to ilmenite inclusions (Fig. 3b). These empty cracks probably were filled by ilmenite inclusions initially, and ilmenite inclusions were replaced by sphene, and sphene was removed afterwards by hydrothermal fluid.

3. Analysis methods

Whole rocks of the representative samples were ground in an agate mill, after careful washing in distilled water. Major elements were measured by XRF spectrometer on glass disks made by fusion of whole rock with lithium metaborate in Waseda University. Precision is 0.5% for element oxides. Analytical data are given in Table 1.

Mineral analyses were carried out by wavelength dispersive X-ray spectrometry on a JEOL Super-probe 8900 electron microprobe at Waseda University. The special filament (LaB_6) was used to maintain constant conditions over a long time. The operation conditions were set to 15 kV and 20 nA using a beam defocused to 10 μm (for some very small mineral phases, a beam defocused to 1 μm was used) with counting time of 10 s for every element. Synthetic pure oxides were used as standards. Pyroxene nomenclature and site assignments follow IMA guidelines (Morimoto, 1989). X-ray mapping was performed to reveal the compositional texture of the Ti–magnetite phenocryst and groundmass using the Super-probe 8900. The operation conditions were set to 15 kV and 20 nA using a beam focused close to 1 μm in order to get a clear image. Dwell time for each point is 20–30 ms. Number of pixels in each image is set to 500–600 with pixel size of 0.01–0.1 μm.

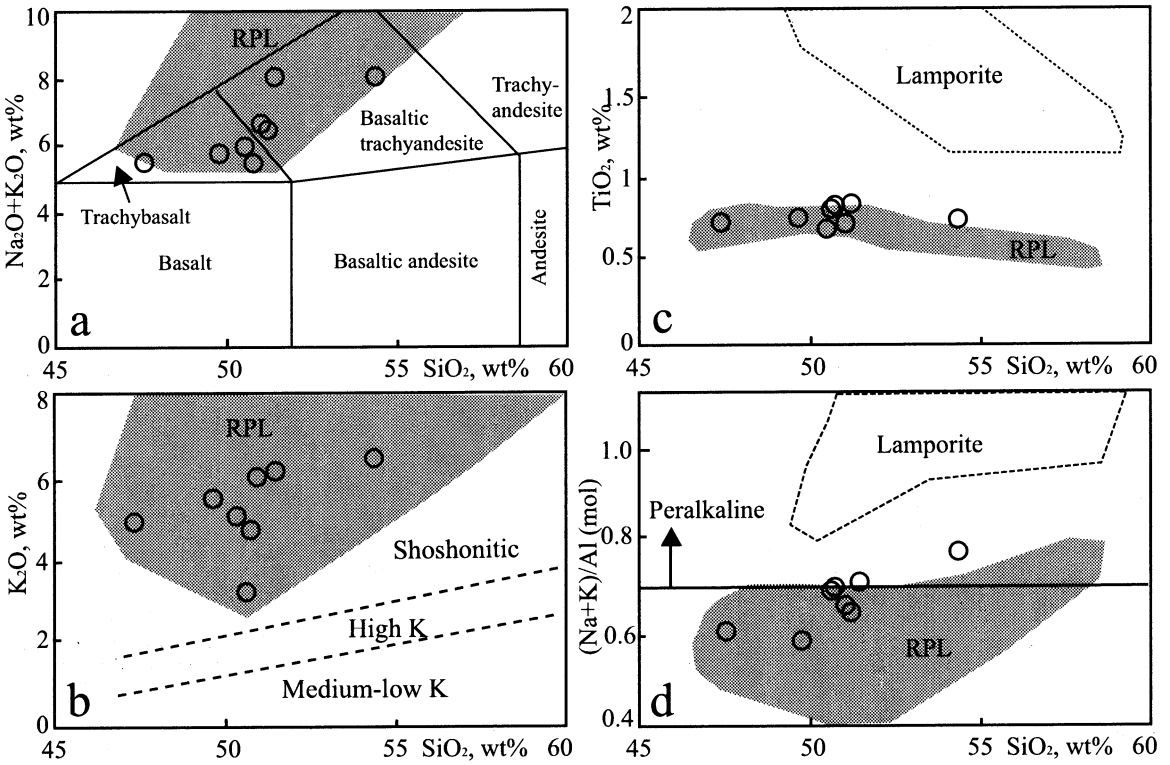

Fig. 4. Total alkali-silica (a) and K_2O (b) versus SiO_2 diagrams after Le Maitre et al. (1989); SiO_2 versus TiO_2 (c) and (Na+K)/Al (d) plots showing the difference between the studied rocks and lamproites, but it is similar to the RPL. Lamproite area is based on Bergman (1987), RPL area is modified from Mitchell and Bergman, 1991 (fig. 6.32, p. 213).

4. Results

4.1. Whole-rock geochemistry

The chemical compositions of the representative samples of Kokchetav 'lamproite' are simply classified as trachybasalt (potassic trachybasalt) and basaltic trachyandesite (shoshonite) (Fig. 4a) according to the TAS diagram by Le Maitre et al. (1990). All samples belong to the shoshonitic group characterized with especially high K_2O contents in the diagram of K_2O versus SiO_2 (Fig. 4b),

Table 1
The representative compositions of Kokchetav 'lamproite'

Oxides, wt%	J527	J530	J525	J522	J533	J534	J537	R120
SiO_2	49.82	50.72	51.45	47.53	51.25	51.08	50.46	54.36
TiO_2	0.76	0.84	0.86	0.76	0.84	0.78	0.69	0.76
Al_2O_3	11.15	10.57	13.70	10.59	12.11	11.11	9.50	12.50
FeO	12.40	11.38	10.65	11.37	10.43	10.34	10.00	9.04
MnO	0.19	0.17	0.17	0.20	0.17	0.16	0.16	0.13
MgO	9.70	8.34	5.96	8.82	8.07	8.77	7.40	5.85
CaO	10.10	12.25	9.04	15.07	10.85	10.70	15.75	8.84
Na_2O	0.36	2.37	1.95	0.70	1.66	0.44	0.84	1.60
K_2O	5.47	3.16	6.09	4.83	4.74	6.03	5.10	6.42
P_2O_5	0.48	0.58	0.55	0.50	0.48	0.51	0.49	0.50
Total	100.43	100.38	100.42	100.37	100.60	99.92	100.39	100.00

Table 2
The representative compositions of clinopyroxene cores

Oxides, wt%	25	26	27	28	29	30	31	32	33	34	35	36	96	126	127	314	315	316	216	251	252	254	255
SiO_2	51.89	52.10	52.31	52.68	52.85	53.38	53.02	52.95	52.84	52.84	52.61	52.9	52.17	53.43	53.34	51.9	51.96	51.85	52.51	52.47	53.48	51.63	52.38
TiO_2	0.63	0.29	0.2	0.34	0.31	0.34	0.31	0.25	0.28	0.32	0.4	0.35	0.48	0.37	0.40	0.50	0.43	0.50	0.41	0.52	0.47	0.62	0.63
Al_2O_3	2.17	1.68	1.63	1.69	1.63	1.69	1.68	1.42	1.39	1.82	2.11	2.06	2.16	1.35	1.42	2.66	2.38	2.53	2.17	2.39	2.18	3.13	2.98
MgO	15.14	16.2	16.11	16.37	16.08	16.4	16.16	16.26	16.34	16.04	16.08	15.33	14.42	16.2	16.24	15.69	15.85	15.64	15.06	15.59	15.8	15.2	15.61
MnO	0.10	0.14	0.15	0.19	0.14	0.17	0.13	0.12	0.15	0.16	0.18	0.15	0.22	0.12	0.19	0.07	0.08	0.06	0.17	0.13	0.13	0.19	0.12
FeO	5.99	5.45	5.35	5.54	5.64	5.57	5.13	5.33	5.15	5.3	5.86	5.69	7.55	5.50	5.44	4.29	4.41	4.68	7.22	5.38	4.72	7.15	6.20
Cr_2O_3	0.17	0.09	0.03	0.07	0.12	0.07	0.03	0.11	0.08	0.09	0.11	0.12	0.01	0.07	0.04	0.67	0.46	0.21	0.01	0.12	0.09	0.06	0.20
CaO	23.33	22.61	22.89	22.90	23.00	23.21	22.98	22.8	22.59	22.44	22.88	22.84	23.14	23.12	23.36	23.63	23.72	23.82	23.11	21.66	23.39	22.48	22.63
Na_2O	0.13	0.12	0.15	0.16	0.16	0.11	0.14	0.15	0.15	0.16	0.14	0.13	0.29	0.14	0.14	0.12	0.15	0.12	0.13	0.13	0.14	0.16	0.14
K_2O	0.01	0	0	0.01	0	0.02	0	0	0	0	0.01	0	0.02	0.01	0.01	0	0.01	0	0	0.02	0	0	0
Total	99.56	98.68	98.82	99.95	99.93	100.96	99.58	99.39	98.97	99.17	100.38	99.57	100.46	100.31	100.58	99.53	99.45	99.41	100.79	98.41	100.4	100.62	100.89
Cation (O=6)																							
Si	1.926	1.942	1.947	1.94	1.947	1.945	1.954	1.957	1.959	1.954	1.931	1.953	1.930	1.958	1.951	1.915	1.92	1.919	1.932	1.951	1.95	1.902	1.910
Ti	0.018	0.008	0.006	0.009	0.009	0.009	0.009	0.007	0.008	0.009	0.011	0.01	0.013	0.01	0.011	0.014	0.012	0.014	0.011	0.015	0.013	0.017	0.017
Al^{IV}	0.074	0.058	0.053	0.06	0.053	0.055	0.047	0.043	0.042	0.046	0.07	0.047	0.07	0.042	0.049	0.085	0.08	0.081	0.068	0.049	0.05	0.099	0.086
Al^{VI}	0.021	0.016	0.018	0.013	0.017	0.018	0.026	0.018	0.019	0.033	0.022	0.043	0.024	0.016	0.012	0.031	0.023	0.029	0.026	0.056	0.044	0.037	0.042
Mg	0.837	0.899	0.893	0.898	0.882	0.89	0.887	0.895	0.902	0.883	0.879	0.843	0.794	0.884	0.885	0.862	0.872	0.862	0.825	0.863	0.858	0.834	0.849
Mn	0.003	0.004	0.005	0.006	0.004	0.005	0.004	0.004	0.005	0.005	0.006	0.005	0.007	0.004	0.006	0.002	0.003	0.002	0.005	0.004	0.004	0.006	0.004
Fe	0.185	0.169	0.166	0.170	0.173	0.169	0.158	0.164	0.159	0.163	0.179	0.175	0.233	0.168	0.166	0.132	0.136	0.144	0.221	0.167	0.143	0.22	0.189
Cr	0.005	0.003	0.001	0.002	0.003	0.002	0.001	0.003	0.002	0.003	0.003	0.003	0.001	0.002	0.001	0.020	0.014	0.006	0.001	0.004	0.003	0.002	0.006
Ca	0.928	0.903	0.913	0.903	0.908	0.906	0.907	0.903	0.897	0.889	0.900	0.904	0.917	0.908	0.915	0.934	0.939	0.944	0.911	0.863	0.914	0.887	0.886
Na	0.010	0.009	0.011	0.012	0.011	0.008	0.01	0.01	0.011	0.012	0.010	0.009	0.021	0.010	0.010	0.008	0.011	0.009	0.010	0.009	0.010	0.011	0.010
K	0.001	0	0	0	0	0.001	0	0	0	0	0.001	0	0.001	0.001	0.001	0	0	0	0	0.001	0	0	0
$Mg^{\#}$	81.6	83.8	84.0	83.6	83.3	83.6	84.6	84.2	84.6	84.0	82.6	82.4	76.8	83.7	83.8	86.5	86.3	85.5	78.4	83.5	85.3	78.7	81.5
En	42.91	45.61	45.28	45.54	44.94	45.27	45.44	45.61	46.05	45.63	44.89	43.86	40.86	45.1	45	44.71	44.8	44.19	42.15	45.6	44.8	42.97	44.13
Wo	47.59	45.8	46.3	45.84	46.25	46.12	46.49	46.03	45.82	45.94	45.95	47.03	47.17	46.32	46.56	48.44	48.24	48.42	46.54	45.59	47.72	45.72	46.05
Fs	9.50	8.59	8.42	8.62	8.82	8.61	8.07	8.37	8.13	8.43	9.16	9.11	11.98	8.57	8.43	6.84	6.97	7.4	11.31	8.81	7.48	11.31	9.81

Table 2 (*Continued*).
The representative compositions of clinopyroxene cores

Oxides, wt%	256	257	259	301	425	426	258	312	313	317	318	319	320	321	322	427	428	431	432	433	434
SiO_2	52.95	52.71	52.16	51.71	52.13	52.57	52.38	51.58	51.95	52.65	52.78	52.85	52.98	52.74	53.08	54.11	53.60	53.99	53.44	53.82	54.73
TiO_2	0.59	0.42	0.48	0.49	0.46	0.61	0.50	0.47	0.45	0.39	0.37	0.31	0.35	0.41	0.29	0.28	0.29	0.23	0.28	0.28	0.22
Al_2O_3	2.75	2.65	2.94	2.58	2.75	2.95	2.77	2.36	2.4	2.16	2.06	1.98	1.91	2.20	1.82	1.41	1.76	1.07	1.61	1.66	1.15
MgO	15.82	15.96	15.46	14.59	15.92	15.54	15.53	15.71	15.84	16.28	16.67	16.03	16.54	16.12	16.43	17.37	17.09	17.92	17.13	16.62	17.18
MnO	0	0.08	0.19	0.17	0.12	0.16	0.12	0.1	0.15	0.12	0.10	0.07	0.09	0.10	0.08	0.07	0.23	0.13	0.14	0.17	0.21
FeO	5.68	5.53	5.92	7.50	4.78	4.8	5.64	4.01	4.53	3.82	3.69	3.46	3.77	4.48	3.41	3.20	3.45	3.98	3.43	3.57	3.94
Cr_2O_3	0.13	0.21	0.07	0.04	0.24	0.07	0.09	0.96	0.78	0.44	0.75	1.07	0.83	0.35	0.64	0.75	0.87	0.32	0.83	0.66	0.32
CaO	21.75	23.05	22.05	22.74	22.12	22.13	22.52	23.39	23.61	23.84	23.79	23.96	23.77	23.76	23.81	21.39	21.31	22.28	22.98	23.21	21.5
Na_2O	0.14	0.14	0.13	0.18	0.14	0.15	0.16	0.19	0.19	0.10	0.13	0.18	0.13	0.14	0.11	0.15	0.09	0.11	0.11	0.13	0.13
K_2O	0.01	0.01	0.01	0.05	0	0	0	0.01	0.01	0	0	0	0.01	0	0	0	0	0	0.01	0	0.01
Total	99.82	100.76	99.41	100.05	98.66	98.98	99.71	98.78	99.91	99.8	100.34	99.91	100.38	100.3	99.67	98.73	98.69	100.03	99.96	100.12	99.39
Cation (O=6)																					
Si	1.941	1.924	1.928	1.919	1.933	1.94	1.93	1.917	1.914	1.932	1.927	1.937	1.934	1.93	1.946	1.982	1.969	1.966	1.950	1.960	1.996
Ti	0.016	0.012	0.013	0.014	0.013	0.017	0.014	0.013	0.012	0.011	0.010	0.009	0.010	0.011	0.008	0.008	0.008	0.006	0.008	0.008	0.006
Al^{IV}	0.059	0.076	0.072	0.081	0.067	0.06	0.07	0.083	0.087	0.068	0.073	0.063	0.067	0.07	0.054	0.018	0.031	0.034	0.050	0.040	0.004
Al^{VI}	0.060	0.038	0.056	0.032	0.053	0.068	0.05	0.02	0.017	0.026	0.015	0.022	0.015	0.025	0.024	0.043	0.046	0.012	0.019	0.031	0.045
Mg	0.864	0.867	0.851	0.806	0.879	0.854	0.852	0.869	0.869	0.890	0.906	0.874	0.899	0.878	0.897	0.947	0.935	0.972	0.931	0.901	0.933
Mn	0	0.002	0.006	0.005	0.004	0.005	0.004	0.003	0.005	0.004	0.003	0.002	0.003	0.003	0.003	0.002	0.007	0.004	0.004	0.005	0.007
Fe	0.174	0.168	0.182	0.232	0.148	0.147	0.173	0.124	0.139	0.117	0.112	0.106	0.115	0.137	0.104	0.098	0.106	0.121	0.104	0.108	0.120
Cr	0.004	0.006	0.002	0.001	0.007	0.002	0.003	0.028	0.023	0.013	0.022	0.031	0.024	0.01	0.018	0.022	0.025	0.009	0.024	0.019	0.009
Ca	0.854	0.902	0.873	0.905	0.879	0.875	0.889	0.932	0.932	0.937	0.930	0.941	0.930	0.932	0.935	0.839	0.839	0.869	0.898	0.906	0.840
Na	0.010	0.010	0.009	0.013	0.010	0.011	0.012	0.014	0.014	0.007	0.009	0.012	0.009	0.01	0.008	0.01	0.007	0.008	0.008	0.009	0.009
K	0	0	0.001	0.002	0	0	0	0.001	0.001	0	0	0	0	0	0	0	0	0	0	0	0
$Mg^{\#}$	83.3	83.6	81.9	77.3	85.3	84.8	82.8	87.2	85.8	88.1	88.7	89.0	88.4	86.3	89.4	90.5	89.3	88.6	89.5	88.8	88.1
En	45.66	44.77	44.64	41.5	46.12	45.51	44.51	45.15	44.79	45.77	46.49	45.53	46.26	45.13	46.32	50.26	49.75	49.53	48.14	47.06	49.29
Wo	45.16	46.54	45.8	46.56	46.12	46.64	46.44	48.4	48.04	48.22	47.74	48.97	47.84	47.86	48.3	44.55	44.64	44.32	46.46	47.29	44.39
Fs	9.18	8.69	9.56	11.94	7.75	7.86	9.05	6.45	7.16	6.01	5.77	5.51	5.9	7.02	5.38	5.18	5.61	6.15	5.4	5.65	6.33

Table 2 (*Continued*).
The representative compositions of clinopyroxene cores

Oxides, wt%	57	58	59	199	201	242	243	248	249	323	326	327	844
SiO_2	48.79	50.04	49.90	50.48	50.04	50.01	50.48	50.34	50.29	49.22	50.26	50.95	49.80
TiO_2	1.03	0.89	0.91	0.64	0.77	0.66	0.62	0.69	0.80	0.85	0.69	0.67	0.87
Al_2O_3	5.14	4.82	4.99	3.72	4.43	4.54	3.84	4.66	4.55	4.58	3.73	3.68	4.70
MgO	13.38	13.54	13.36	13.89	13.25	12.74	13.12	13.47	13.27	12.96	13.76	13.71	13.18
MnO	0.14	0.21	0.19	0.15	0.17	0.25	0.28	0.27	0.25	0.19	0.18	0.21	0.24
FeO	8.84	8.73	8.99	7.45	8.22	8.91	8.76	7.81	8.58	8.05	7.45	7.79	8.81
Cr_2O_3	0.04	0.03	0.05	0.02	0.03	0.03	0.05	0.05	0.06	0.02	0.04	0.02	0.01
CaO	22.20	22.33	22.24	23.17	22.89	23.24	23.48	22.47	21.7	22.86	22.96	22.86	21.45
Na_2O	0.24	0.20	0.20	0.21	0.28	0.18	0.19	0.21	0.18	0.26	0.38	0.38	0.24
K_2O	0	0.01	0.02	0.02	0.03	0.02	0.01	0.14	0.03	0.01	0	0.01	0.02
Total	99.80	100.80	100.85	99.75	100.11	100.58	100.83	100.11	99.71	99.00	99.45	100.28	99.32
Cation (O=6)													
Si	1.831	1.854	1.85	1.884	1.866	1.865	1.878	1.871	1.878	1.858	1.881	1.890	1.870
Ti	0.029	0.025	0.025	0.018	0.022	0.019	0.017	0.019	0.022	0.024	0.019	0.019	0.025
Al^{IV}	0.169	0.146	0.150	0.116	0.134	0.135	0.122	0.129	0.122	0.142	0.120	0.110	0.131
Al^{VI}	0.058	0.064	0.068	0.047	0.060	0.064	0.045	0.075	0.078	0.061	0.045	0.051	0.077
Mg	0.747	0.747	0.737	0.772	0.736	0.707	0.726	0.746	0.738	0.728	0.766	0.757	0.736
Mn	0.004	0.006	0.006	0.005	0.005	0.008	0.009	0.008	0.008	0.006	0.006	0.006	0.008
Fe	0.276	0.270	0.278	0.232	0.255	0.277	0.271	0.242	0.267	0.253	0.232	0.241	0.276
Cr	0.001	0.001	0.001	0.001	0.001	0.001	0.002	0.001	0.002	0.001	0.001	0.001	0
Ca	0.893	0.887	0.884	0.926	0.915	0.928	0.936	0.895	0.869	0.924	0.920	0.908	0.863
Na	0.018	0.015	0.014	0.015	0.02	0.013	0.014	0.015	0.013	0.019	0.027	0.027	0.017
K	0	0.001	0.001	0.001	0.001	0.001	0	0.007	0.002	0	0	0.001	0.001
$Mg^{\#}$	72.7	73.0	72.2	76.5	73.8	71.3	72.2	74.9	72.8	73.7	76.3	75.4	72.2
En	38.99	39.25	38.83	39.99	38.60	36.97	37.57	39.61	39.39	38.21	39.93	39.72	39.29
Wo	46.58	46.59	46.54	48.01	47.99	48.55	48.39	47.54	46.35	48.5	47.96	47.65	46.02
Fs	14.42	14.16	14.64	12	13.4	14.48	14.04	12.85	14.26	13.29	12.1	12.63	14.7

$Mg^{\#} = 100\ Mg/(Mg+Fe)$.

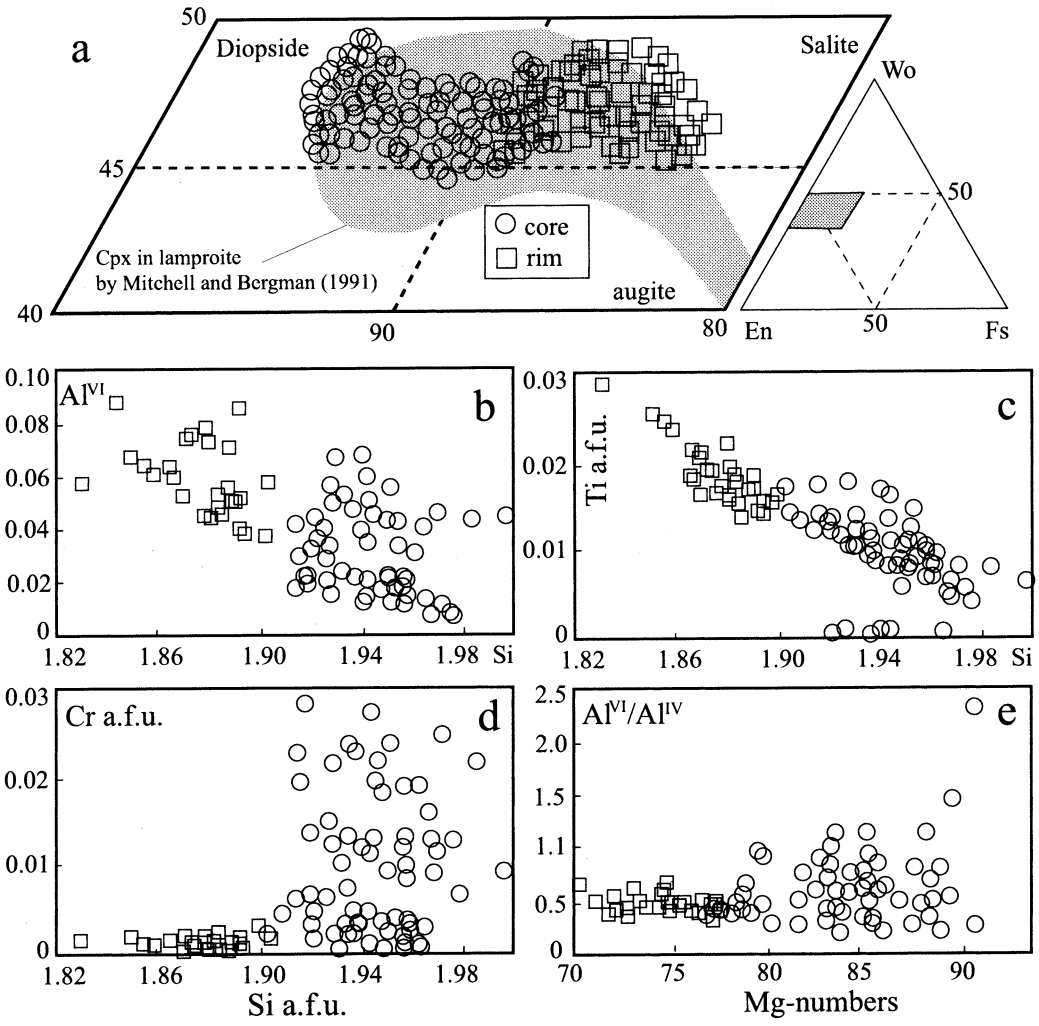

Fig. 5. (a) The Wo–En–Fs diagrams showing the compositions of clinopyroxene phenocryst in Kokchetav 'lamproite'. The compositional spaces of the representative lamproite clinopyroxene (by Mitchell and Bergman, 1991) are compiled for comparison; b–e) Plots of Si versus Al^{VI} (b), Ti (c) and Cr (d) show the variances of clinopyroxene compositions; (e) plot of Al^{VI}/Al^{IV} ratios versus Mg-numbers.

and completely correspond to Roman Province lava (RPL) in both diagrams.

Very high FeO (9–12.4%) and CaO contents (8.8–15.1%) of the studied rocks made it difficult to classify these rocks. Although high CaO content could be due to the clinopyroxene accumulation as these rocks contain abundant clinopyroxene phenocrysts, but lower MgO contents (5.9–9.7%) do not support this explanation. Comparing with typical lamprites (Bergman, 1987; Mitchell and Bergman, 1991), Kokchetav 'lamproites' are poor in TiO_2 (0.69–0.86 wt%, Table 1), which is totally consistent with the RPL in the SiO_2–TiO_2 plot (Fig. 4c). This is further proved in (Na+K)/Al–SiO_2 plot although one sample locates outside of the RPL field (Fig. 4d).

It is clear that the Kokchetav 'lamproite' is not lamproite, but a kind of shoshonitic rock, which highly resembles the RPL in bulk composition.

Table 3
The chemical compositions of clinopyroxene crystal I from its rim to core to rim

Oxides, wt%	rim	rim	rim	rim	rim	core	core	core	core	core	core	core	core	core	core	core	core	rim	rim	rim	rim	rim
SiO_2	49.80	49.86	49.86	49.71	48.54	52.12	52.66	52.37	51.93	51.93	52.02	52.45	52.51	52.94	53.15	52.68	51.60	49.4	49.68	50.29	49.84	49.79
TiO_2	0.87	0.83	0.78	0.75	0.60	0.43	0.40	0.50	0.31	0.35	0.43	0.42	0.51	0.40	0.35	0.35	0.45	0.48	0.58	0.65	0.70	0.80
Al_2O_3	4.70	4.63	4.36	4.59	5.72	2.44	2.14	2.33	2.66	2.63	2.56	2.47	2.40	1.87	1.78	2.32	2.83	4.73	4.59	4.39	4.40	4.44
MgO	13.18	13.37	13.4	13.12	12.74	15.94	16.67	16.14	15.7	15.88	15.66	15.71	16.16	16.59	16.49	15.94	15.27	12.98	13.17	13.31	13.32	13.17
MnO	0.24	0.16	0.17	0.17	0.18	0.09	0.06	0.06	0.07	0.05	0.06	0.06	0.09	0.05	0.10	0.11	0.07	0.17	0.19	0.15	0.20	0.16
FeO	8.81	8.34	8.35	8.43	8.83	4.96	3.90	4.11	4.94	4.87	4.62	4.68	4.59	3.78	3.95	4.69	5.77	8.76	8.57	8.78	8.61	8.66
Cr_2O_3	0.01	0	0.02	0.03	0.06	0.42	0.95	0.66	0.30	0.51	0.79	0.45	0.52	0.75	0.55	0.40	0.16	0	0	0.02	0.01	0.03
CaO	21.45	22.96	21.67	22.87	21.64	23.24	22.34	22.57	22.16	22.89	22.54	22.84	23.76	23.3	22.47	23.33	23.23	22.06	21.07	21.81	22.32	21.83
Na_2O	0.24	0.31	0.25	0.28	0.26	0.20	0.18	0.17	0.13	0.21	0.20	0.18	0.15	0.18	0.14	0.18	0.17	0.34	0.27	0.25	0.29	0.26
K_2O	0.02	0	0.01	0	0	0	0	0	0.01	0.01	0	0	0	0	0	0	0	0.01	0	0.01	0.01	0.02
Total	99.32	100.46	98.87	99.95	98.57	99.84	99.30	98.91	98.21	99.33	98.88	99.26	100.69	99.86	98.98	100.00	99.55	98.93	98.12	99.66	99.7	99.16
Cation (O=6)																						
Si	1.870	1.854	1.877	1.859	1.840	1.920	1.936	1.935	1.936	1.919	1.928	1.936	1.917	1.938	1.958	1.933	1.913	1.865	1.883	1.881	1.867	1.873
Ti	0.025	0.023	0.022	0.021	0.017	0.012	0.011	0.014	0.009	0.01	0.012	0.012	0.014	0.011	0.010	0.010	0.013	0.014	0.017	0.018	0.020	0.023
Al^{IV}	0.131	0.146	0.123	0.141	0.16	0.081	0.064	0.065	0.064	0.081	0.072	0.064	0.083	0.062	0.043	0.067	0.088	0.135	0.118	0.120	0.133	0.127
Al^{VI}	0.077	0.057	0.07	0.061	0.095	0.025	0.028	0.036	0.053	0.034	0.039	0.043	0.020	0.019	0.035	0.033	0.036	0.075	0.087	0.074	0.061	0.069
Mg	0.736	0.740	0.751	0.73	0.719	0.874	0.912	0.888	0.871	0.874	0.864	0.863	0.878	0.904	0.904	0.871	0.843	0.729	0.743	0.741	0.743	0.737
Mn	0.008	0.005	0.005	0.006	0.006	0.003	0.002	0.002	0.002	0.002	0.002	0.002	0.003	0.002	0.003	0.003	0.002	0.005	0.006	0.005	0.006	0.005
Fe	0.276	0.258	0.262	0.263	0.279	0.152	0.120	0.127	0.154	0.150	0.143	0.144	0.140	0.115	0.121	0.143	0.178	0.276	0.271	0.274	0.269	0.272
Cr	0	0	0.001	0.001	0.002	0.012	0.028	0.019	0.009	0.015	0.023	0.013	0.015	0.022	0.016	0.012	0.005	0	0	0.001	0.001	0.001
Ca	0.863	0.915	0.874	0.916	0.879	0.917	0.880	0.894	0.885	0.907	0.895	0.903	0.929	0.914	0.887	0.917	0.923	0.892	0.856	0.874	0.896	0.880
Na	0.017	0.022	0.018	0.020	0.019	0.014	0.013	0.012	0.010	0.015	0.014	0.013	0.011	0.013	0.01	0.013	0.012	0.025	0.02	0.018	0.021	0.019
K	0.001	0	0.001	0	0	0	0	0	0	0.001	0	0	0	0	0	0	0	0.001	0.001	0.001	0.001	0.001
$Mg^{\#}$	72.2	73.8	73.7	73.1	71.6	84.9	88.3	87.4	84.8	85.2	85.7	85.6	86.1	88.6	87.9	85.6	82.4	72.2	72.9	72.7	73.0	72.7
En	39.29	38.69	39.81	38.25	38.31	44.97	47.73	46.53	45.61	45.27	45.44	45.19	45.11	46.77	47.28	45.10	43.36	38.45	39.74	39.24	38.94	39.04
Wo	46.02	47.81	46.31	47.99	46.83	47.19	46.02	46.84	46.35	46.95	47.05	47.28	47.73	47.27	46.38	47.48	47.47	47.03	45.78	46.27	46.97	46.58
Fs	14.70	13.50	13.88	13.76	14.86	7.84	6.25	6.63	8.04	7.77	7.50	7.53	7.16	5.96	6.34	7.42	9.17	14.52	14.48	14.48	14.10	14.38

Table 3 (*Continued*).
The chemical compositions of clinopyroxene crystal II from its rim to core to rim

Oxides, wt%	rim	→							core											rim
SiO_2	49.82	49.80	50.56	50.22	52.43	53.00	52.97	53.78	53.58	53.41	53.01	53.88	53.02	53.09	52.91	52.77	50.31	50.69	49.90	50.33
TiO_2	0.60	0.49	0.52	0.66	0.29	0.28	0.23	0.15	0.16	0.18	0.21	0.19	0.26	0.24	0.23	0.20	0.51	0.51	0.59	0.60
Al_2O_3	4.13	3.72	3.63	3.72	1.88	1.53	1.46	0.78	0.95	1.10	1.30	0.87	1.54	1.47	1.56	1.74	3.30	3.49	4.15	3.80
MgO	12.76	13.45	14.05	13.95	16.17	16.66	16.38	17.15	17.51	16.94	16.61	17.18	16.17	16.26	16.18	15.96	14.23	14.02	13.70	13.87
MnO	0.12	0.16	0.17	0.17	0.15	0.16	0.14	0.20	0.21	0.20	0.11	0.12	0.12	0.12	0.11	0.2	0.22	0.2	0.20	0.20
FeO	7.50	7.86	7.52	7.49	4.56	3.40	3.38	3.26	3.08	3.27	3.66	3.29	3.63	3.88	3.89	4.38	7.17	6.53	7.60	6.73
Cr_2O_3	0.02	0	0	0.07	0.16	0.31	0.44	0.23	0.40	0.43	0.34	0.44	0.65	0.41	0.28	0.14	0	0.04	0	0.04
CaO	23.12	22.84	22.68	22.8	23.48	23.84	23.87	23.66	23.31	23.48	23.8	23.51	23.77	23.9	23.75	23.6	22.86	22.93	23.09	23.18
Na_2O	0.21	0.27	0.22	0.18	0.14	0.15	0.12	0.09	0.07	0.14	0.18	0.08	0.16	0.13	0.13	0.14	0.21	0.20	0.26	0.21
K_2O	0	0	0	0	0	0	0	0.02	0	0	0	0	0	0.01	0	0.02	0	0	0	0
Total	98.28	98.59	99.35	99.26	99.26	99.33	98.99	99.32	99.27	99.15	99.22	99.56	99.32	99.51	99.03	99.15	98.81	98.61	99.49	98.96
Cation (O=6)																				
Si	1.887	1.884	1.892	1.883	1.939	1.95	1.955	1.975	1.967	1.965	1.954	1.973	1.953	1.954	1.955	1.952	1.893	1.903	1.869	1.888
Ti	0.017	0.014	0.015	0.019	0.008	0.008	0.006	0.004	0.004	0.005	0.006	0.005	0.007	0.007	0.006	0.006	0.014	0.014	0.017	0.017
Al^{IV}	0.113	0.116	0.108	0.117	0.061	0.05	0.045	0.025	0.033	0.035	0.046	0.027	0.047	0.046	0.045	0.048	0.107	0.097	0.131	0.112
Al^{VI}	0.071	0.050	0.052	0.047	0.021	0.016	0.019	0.008	0.008	0.013	0.011	0.010	0.020	0.017	0.023	0.027	0.039	0.058	0.052	0.055
Mg	0.720	0.758	0.783	0.779	0.89	0.912	0.901	0.938	0.957	0.928	0.912	0.937	0.886	0.891	0.890	0.879	0.797	0.783	0.764	0.775
Mn	0.004	0.005	0.005	0.005	0.005	0.005	0.004	0.006	0.006	0.006	0.004	0.004	0.004	0.004	0.003	0.006	0.007	0.006	0.006	0.006
Fe	0.237	0.248	0.234	0.234	0.141	0.104	0.104	0.100	0.094	0.101	0.113	0.101	0.111	0.119	0.120	0.135	0.225	0.204	0.237	0.210
Cr	0.001	0	0	0.002	0.005	0.009	0.013	0.007	0.011	0.013	0.010	0.013	0.019	0.012	0.008	0.004	0	0.001	0	0.001
Ca	0.938	0.926	0.909	0.916	0.93	0.94	0.944	0.931	0.917	0.925	0.940	0.922	0.938	0.942	0.940	0.935	0.922	0.922	0.927	0.931
Na	0.016	0.020	0.016	0.013	0.010	0.011	0.009	0.007	0.005	0.010	0.013	0.006	0.011	0.009	0.009	0.010	0.015	0.015	0.019	0.016
K	0	0	0	0	0	0	0	0.001	0	0	0	0	0	0	0	0.001	0	0.001	0	0.001
$Mg^{\#}$	75.0	75.0	76.6	76.5	86.0	89.3	89.3	89.9	90.5	89.7	88.7	90.1	88.5	87.9	87.8	86.2	77.5	78.8	75.8	78.2
En	37.99	39.23	40.64	40.38	45.39	46.64	46.21	47.64	48.62	47.50	46.41	47.81	45.79	45.63	45.64	45.08	41.02	41.02	39.64	40.43
Wo	49.52	47.95	47.2	47.49	47.43	48.04	48.46	47.29	46.59	47.37	47.86	47.07	48.46	48.27	48.22	47.99	47.41	48.29	48.07	48.60
Fs	12.49	12.82	12.17	12.13	7.17	5.32	5.33	5.07	4.79	5.13	5.73	5.12	5.76	6.10	6.14	6.93	11.57	10.69	12.3	10.97

$Mg^{\#} = 100\ Mg/(Mg+Fe)$.

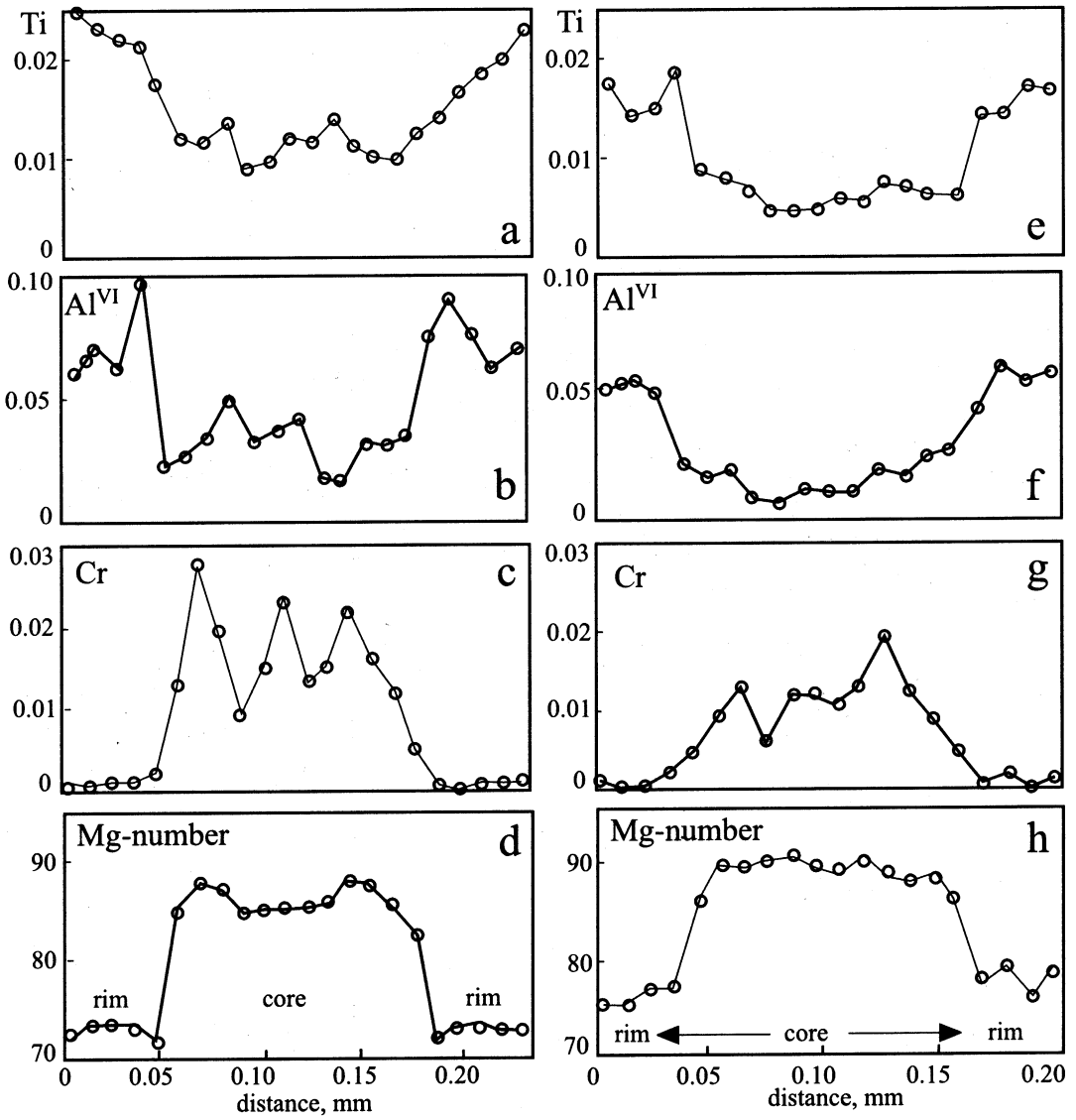

Fig. 6. The compositional profiles for two representative clinopyroxene phenocrysts, (a–d) for crystal I and (e–h) for crystal II (data from Table 3).

4.2. Mineral compositions

4.2.1. Clinopyroxene phenocryst

Clinopyroxene is the most important mineral phase and occurs only as phenocryst in Kokchetav 'lamproite'. The representative clinopyroxene compositions are presented in Tables 2 and 3. Table 3 presents compositions of two representative clinopyroxene crystals. All clinopyroxene analyses display large compositional differences between cores and rims (Fig. 5). Most clinopyroxene cores are diopside and rims are salite (Fig. 5a), and both rims and cores fall into the area defined as lamproite clinopyroxene by Mitchell and Bergman (1991). However, Ti contents are much lower and Al contents are much higher than clinopyroxene in typical lamproites. Si contents roughly correlate with Al^{VI} and Ti (Fig. 5b,c, re-

Table 4
The representative compositions of magnetite cores with abundant ilmenite inclusions

Oxides, wt%	366	367	369	370	373	374	375	380	381	382	383	384	385	386	387	390	396
SiO_2	0.36	0.22	0.11	1.09	0.79	0.85	0.77	0.13	0.13	0.14	0.15	0.68	0.18	0.73	0.61	0.89	0.81
Al_2O_3	3.29	2.86	5.07	3.17	1.98	1.98	1.82	3.58	5.15	3.71	5.67	3.99	1.31	1.33	1.23	0.55	0.56
TiO_2	6.22	5.86	5.51	5.50	4.30	3.46	2.94	5.89	7.21	5.24	6.99	4.94	4.78	3.75	4.27	3.75	3.35
FeO^a_{cal}	22.89	25.88	17.12	7.51	23.06	15.42	9.13	3.29	15.29	30.23	40.36	18.10	14.94	10.16	8.67	16.80	20.00
$Fe_2O^a_3$cal	66.30	64.40	71.52	81.64	69.07	77.32	84.46	86.47	71.37	59.85	45.50	71.58	77.69	83.14	84.34	77.45	74.71
MnO	0.32	0.28	0.09	0.20	0.10	0.16	0.14	0.09	0.26	0.14	0.28	0.05	0.04	0.14	0.40	0.11	0.10
Cr_2O_3	0.12	0.09	0.08	0.15	0.13	0.16	0.10	0.08	0.04	0.08	0	0.08	0.01	0.03	0.04	0.08	0.027
MgO	0.14	0.06	0.04	0.22	0.13	0.19	0.19	0.04	0.06	0.05	0.59	0.06	0.02	0.22	0.12	0.04	0.04
CaO	0	0	0	0.240	0.14	0.15	0.13	0	0	0	0	0	0.35	0.27	0.07	0.13	0.24
V_2O_3	0.32	0.35	0.41	0.27	0.32	0.31	0.32	0.43	0.47	0.51	0.45	0.46	0.28	0.23	0.25	0.16	0.18
P_2O_5	0.04	0	0.05	0.02	0	0	0.01	0	0.03	0.04	0	0.05	0.40	0	0	0	0
Total	100	100	100	100	100	100	100	100	100	100	100	100	100	100	100	100	100
FeO_{Total}	82.54	83.82	81.48	80.98	85.20	84.99	85.12	81.10	79.51	84.09	81.31	82.51	84.84	84.97	84.56	86.52	87.22
Cation ($O=4$)																	
Si	0.013	0.008	0.004	0.038	0.029	0.030	0.027	0.004	0.005	0.005	0.006	0.024	0.007	0.026	0.022	0.032	0.030
Al	0.140	0.123	0.211	0.129	0.085	0.084	0.076	0.144	0.212	0.161	0.248	0.167	0.055	0.056	0.051	0.024	0.024
Ti	0.169	0.161	0.146	0.143	0.118	0.093	0.078	0.152	0.189	0.145	0.195	0.132	0.129	0.100	0.113	0.102	0.092
Fe^{2+}	0.689	0.789	0.505	0.217	0.702	0.461	0.269	0.094	0.446	0.930	1.252	0.537	0.447	0.301	0.256	0.508	0.611
Fe^{3+}	1.796	1.768	1.896	2.121	1.892	2.081	2.243	2.230	1.872	1.656	1.270	1.909	2.091	2.216	2.240	2.109	2.055
Mn	0.010	0.009	0.003	0.006	0.003	0.005	0.004	0.003	0.008	0.004	0.009	0.002	0.001	0.004	0.012	0.003	0.003
Cr	0.003	0.003	0.002	0.004	0.004	0.004	0.003	0.002	0.001	0.002	0	0.002	0	0.001	0.001	0.002	0.001
Mg	0.007	0.004	0.002	0.011	0.007	0.010	0.010	0.002	0.003	0.003	0.033	0.003	0.001	0.012	0.006	0.002	0.002
Ca	0	0	0	0.009	0.005	0.006	0.005	0	0	0	0	0	0.013	0.010	0.003	0.005	0.009
V	0.008	0.009	0.009	0.006	0.008	0.007	0.008	0.010	0.011	0.012	0.011	0.011	0.007	0.005	0.006	0.004	0.004
P	0.001	0	0.002	0	0	0	0	0	0.001	0.001	0	0.002	0.012	0	0	0	0
Usp, mol%	7.99	7.83	6.48	5.96	5.61	4.12	3.25	6.00	8.32	7.38	11.39	5.96	5.66	4.21	4.71	4.56	4.24
Sp, mol%	6.79	6.11	9.44	5.55	4.22	3.89	3.27	5.80	9.35	8.30	14.47	7.65	2.44	2.37	2.18	1.16	1.14

FeO_{Total} is directly obtained by microprobe analysis; Usp = ulvöspinel ($Fe_2^{2+}TiO_4$); Sp = spinel ($(Mg,Fe^{2+},Mn,Ca)(Al,Cr)_2O_4$).

[a] Calculated by assuming the absent amounts of content (the difference between the analysis total and 100) are due to the Fe^{3+} in magnetite.

Table 5
The representative composition of magnetite rims

Oxides, wt%	397	398	399	419	404	405	360	362	379	388	389	391	392	393	394	395	401
SiO_2	1.33	0.81	1.07	0.11	1.00	1.09	1.21	0.98	1.04	1.10	0.89	0.81	0.82	1.01	1.06	1.04	0.95
Al_2O_3	1.08	1.18	1.21	0.58	0.66	0.62	0.52	1.07	0.99	1.15	1.13	0.80	0.67	0.63	0.68	0.84	0.80
TiO_2	2.05	2.13	1.65	3.08	1.89	1.98	0.82	1.89	2.40	1.87	2.24	1.68	2.94	1.17	1.14	1.19	1.38
FeO^a_{cal}	29.29	28.75	19.49	20.98	14.15	11.51	25.30	21.03	12.18	12.70	24.34	25.35	15.26	21.44	26.85	27.84	29.65
$Fe_2O^a_3$cal	65.49	66.60	76.07	69.17	81.84	84.32	71.73	74.24	82.67	82.70	70.83	70.84	79.86	75.34	69.81	68.80	66.81
MnO	0.02	0.11	0.05	0.05	0	0.01	0.06	0.13	0.06	0.04	0.02	0.07	0.05	0.08	0.09	0	0.03
Cr_2O_3	0.01	0.02	0	0.04	0.04	0.04	0	0.13	0.14	0.02	0.04	0.04	0.07	0.02	0	0.02	0.04
MgO	0.14	0.08	0.08	0.06	0.03	0.07	0.05	0.16	0.12	0.12	0.14	0.11	0.07	0.06	0.07	0.07	0.09
CaO	0.41	0.14	0.18	2.84	0.21	0.24	0.11	0.17	0.16	0.07	0.12	0.07	0.12	0.09	0.14	0.15	0.15
V_2O_3	0.17	0.15	0.16	0.44	0.16	0.13	0.21	0.20	0.23	0.20	0.25	0.22	0.16	0.16	0.10	0.05	0.13
P_2O_5	0	0.04	0.05	2.66	0.03	0	0	0.005	0.02	0.03	0	0.01	0	0.01	0.07	0	0
Total	100	100	100	100	100	100	100	100	100	100	100	100	100	100	100	100	100
FeO_{Total}	88.23	88.68	87.94	83.21	87.79	87.37	89.84	87.83	86.57	87.12	88.08	89.09	87.11	89.23	89.67	89.74	89.77
Cation ($O=4$)																	
Si	0.050	0.030	0.039	0.004	0.036	0.039	0.045	0.036	0.037	0.040	0.033	0.030	0.029	0.037	0.040	0.039	0.036
Al	0.047	0.052	0.052	0.025	0.028	0.026	0.023	0.046	0.042	0.049	0.049	0.035	0.028	0.028	0.030	0.037	0.035
Ti	0.058	0.060	0.045	0.084	0.051	0.054	0.023	0.052	0.065	0.050	0.062	0.047	0.080	0.033	0.032	0.034	0.039
Fe^{2+}	0.916	0.900	0.595	0.632	0.427	0.345	0.789	0.645	0.364	0.380	0.752	0.789	0.461	0.662	0.840	0.873	0.934
Fe^{3+}	1.842	1.877	2.089	1.875	2.222	2.273	2.013	2.048	2.223	2.228	1.969	1.985	2.170	2.092	1.965	1.941	1.895
Mn	0.001	0.003	0.002	0.002	0	0	0.002	0.004	0.002	0.001	0.001	0.002	0.001	0.002	0.003	0	0.001
Cr	0	0.001	0	0.001	0.001	0.001	0	0.004	0.004	0.001	0.001	0.001	0.002	0.001	0	0.001	0.001
Mg	0.008	0.004	0.005	0.003	0.002	0.004	0.003	0.009	0.007	0.006	0.008	0.006	0.004	0.003	0.004	0.004	0.005
Ca	0.016	0.006	0.007	0.110	0.008	0.009	0.004	0.007	0.006	0.003	0.005	0.003	0.005	0.003	0.005	0.006	0.006
V	0.004	0.004	0.004	0.011	0.004	0.003	0.005	0.005	0.005	0.005	0.006	0.006	0.004	0.004	0.002	0.001	0.003
P	0	0.001	0.002	0.081	0.001	0	0	0	0.001	0.001	0	0	0	0	0.002	0	0
Ulv, mol%	2.95	3.02	2.06	4.21	2.23	2.27	1.12	2.43	2.77	2.17	2.99	2.28	3.50	1.51	1.58	1.67	1.98
Sp, mol%	2.45	2.63	2.37	1.30	1.26	1.15	1.10	2.33	1.95	2.12	2.42	1.76	1.34	1.31	1.47	1.88	1.85

FeO_{Total} is directly obtained by microprobe analysis; Usp = ulvöspinel ($Fe_2^{2+}TiO_4$); Sp = spinel ($(Mg,Fe^{2+},Mn,Ca)(Al,Cr)_2O_4$).

[a] Calculated by assuming the absent amounts of content (the difference between the analysis total and 100) are due to the Fe^{3+} in magnetite.

spectively). Clinopyroxene rims generally are enriched in Al^{VI} and Ti but depleted in Si relative to their cores. Si contents are higher than 1.90 a.f.u. (atomic formula unit) for clinopyroxene cores, and generally lower than 1.90 a.f.u. for clinopyroxene rims. Cr contents are highly variable especially for clinopyroxene cores. Cr contents are higher in cores than in rims. However, there is no correlation between Cr and Si contents (Fig. 5d). Clinopyroxene cores are characterized with high Mg-numbers and high Al^{VI}/Al^{IV} ratios relative to rims (Fig. 5e). Al^{VI}/Al^{IV} ratios for cores range from 0.216 to 2.389 (average = 0.592). These ratios vary between 0.343 and 0.775 in rims (average = 0.476). High Al^{VI}/Al^{IV} ratio is considered to be a characteristic of HP clinopyroxene (Thompson, 1974; Wass, 1979). High Al^{VI}/Al^{IV} ratios in clinopyroxene cores therefore suggest that the Kokchetav clinopyroxene cores crystallized at HP relative to rims.

The discontinuities in chemical composition were evident in clinopyroxene crystals as shown in Fig. 6. These two clinopyroxene crystals have similar zoning patterns with lower Al^{VI} and Ti contents but higher Mg-numbers and Cr contents in cores than rims. All these observations imply different crystallization conditions for clinopyroxene cores and rims.

The complex clinopyroxene structure gives some information to evaluate relative pressure and temperature of clinopyroxene crystallization from Kokchetav 'lamproite' magma. In Ramsay's classification diagram Ramsay (1992), Kokchetav clinopyroxene fall into 'on-craton' garnet–peridotite space and eclogite–pyroxenite–phenocryst space (Fig. 7a). All clinopyroxene rims fall in the lower-pressure eclogite–pyroxenite–phenocryst space, whereas about half clinopyroxene cores fall into the 'on-craton' garnet–peridotite space. This difference implies that clinopyroxene cores crystallized at higher pressure (in mantle) than the rims (in crust). Cr content in clinopyroxene is insensitive to temperature but sensitive to pressure. As Na content is relatively low in clinopyroxene cores, the exchanged Cr component in clinopyroxene must be tschermakitic (e.g. $CaCrAlSiO_6$), in which the excess charge of Cr is balanced by Al substituting for Si in tetrahedral site. Brey et al.

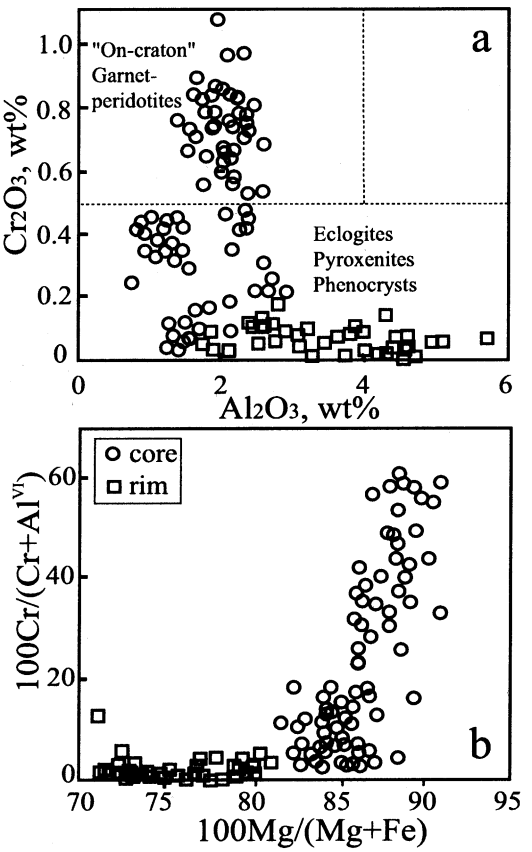

Fig. 7. (a) The Cr_2O_3 versus Al_2O_3 plot for Kokchetav clinopyroxene, discrimination lines are based on Ramsay (1992). (b) Mg-number versus Cr-number plot for clinopyroxene phenocrysts.

(1986) showed a lower effect of temperature on Cr exchange than is the case for exchange of other tschermakitic components in clinopyroxene. Clinopyroxene with high Cr content generally crystallize at HP. Cr content is balanced by Al^{VI} in clinopyroxene structure, and $100Cr/(Cr+Al^{VI})$ ratio (Cr-number) correlates with pressure (Nimis and Taylor, 2000). Cr-number therefore is used to estimate the relative pressure at which clinopyroxene crystallized. Clinopyroxene cores are characterized with high Mg-numbers (>80) and largely variable Cr-numbers (65–3), whereas clinopyroxene rims differ from their cores apparently with low Mg-numbers and Cr-numbers (Fig. 7b). These differences suggest clinopyroxene cores crystallized at high but largely variable pressures,

Table 6
The representative compositions of ilmenite inclusions in magnetite cores and sphene in magnetite cracks

Ilmenite	114	117	358	420	421	Sphene	347	413	414	415	416
SiO_2	0.12	0.11	0.12	0.10	0.10	SiO_2	30.83	30.73	31.95	33.05	32.67
Al_2O_3	2.17	1.48	1.28	1.59	2.58	Al_2O_3	5.18	4.09	4.18	4.73	4.27
TiO_2	42.51	41.98	42.77	43.57	41.10	TiO_2	32.59	32.76	33.23	31.15	32.89
FeO_{Total}	49.46	50.41	50.45	49.15	49.87	FeO_{Total}	1.66	1.69	1.63	1.47	1.49
MnO	1.95	2.73	2.84	2.73	3.90	MnO	0	0.04	0.08	0.04	0.01
Cr_2O_3	0.04	0.05	0.06	0.09	0.06	Cr_2O_3	0.03	0	0	0	0.02
MgO	0.04	0.06	0.07	0.04	0.05	MgO	0.16	0.04	0.03	0.14	0.04
CaO	0	0	0	0.06	0	CaO	28.74	28.48	27.39	27.63	27.89
V_2O_3	0.43	0.31	0.35	0.33	0.36	V_2O_3	0.44	0.42	0.38	0.41	0.39
P_2O_5	0	0.01	0.03	0	0	P_2O_5	0.60	0.02	0	0.71	0
Total	96.72	97.14	97.97	97.66	98.02	Total	100.23	98.27	98.86	99.33	99.67
Cation (O=3)						Cation (O=5)					
Si	0.003	0.003	0.003	0.003	0.002	Si	1.009	1.022	1.048	1.080	1.062
Al	0.066	0.045	0.038	0.047	0.075	Al	0.200	0.160	0.162	0.182	0.164
Ti	0.828	0.809	0.816	0.829	0.767	Ti	0.803	0.820	0.820	0.766	0.805
Fe	1.071	1.080	1.070	1.039	1.035	Fe	0.045	0.047	0.045	0.040	0.041
Mn	0.160	0.221	0.228	0.218	0.306	Mn	0	0.004	0.008	0.004	0.001
Cr	0.001	0.001	0.001	0.002	0.001	Cr	0.001	0	0	0	0.001
Mg	0.002	0.002	0.003	0.002	0.002	Mg	0.008	0.002	0.001	0.007	0.002
Ca	0	0	0	0.002	0	Ca	1.008	1.015	0.963	0.968	0.978
V	0.009	0.006	0.007	0.007	0.007	V	0.012	0.011	0.010	0.011	0.010
P	0	0	0.001	0	0	P	0.021	0.001	0	0.025	0

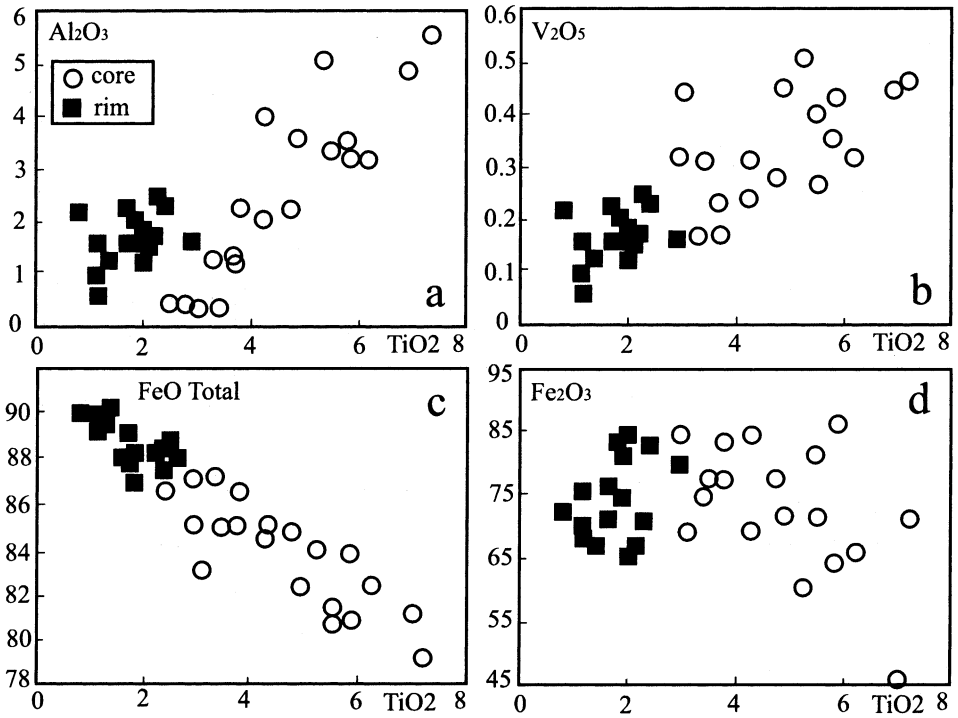

Fig. 8. Plots of several major elements showing magnetite compositions.

and clinopyroxene rims formed at lower pressures.

4.2.2. Ti–magnetite compositions and T-fO_2 conditions

Representative magnetite analyses present in Table 4 (cores) and Table 5 (rims). As ilmenite inclusions are very small in size, relatively few analyses were obtained by electronic probe. Representative ilmenite and sphene compositions are listed in Table 6. In order to calculate Fe_2O_3 contents in magnetite, we assumed that the difference between the analysis total and 100% is only due to the occurrence of Fe^{3+}.

Magnetite cores differ from their rims mainly in TiO_2 content. TiO_2 contents in magnetite cores are higher than in their rims (Fig. 8). The ulvöspinel component varies between 3.25 and 11.39 mol% (average 6.09%) in magnetite core (Table 4), whereas between 1.51 and 4.21% (average 2.40%) in the magnetite rim (Table 5). Magnetite cores are characterized by high and largely variable TiO_2, Al_2O_3, V_2O_5 (Fig. 8a,b), but low total FeO contents (Fig. 8c). The calculated Fe_2O_3 contents are not significantly different from the cores to rims (Fig. 8d). Magnetite SiO_2 contents are low and cores and rims are similar (0.11–1.09 wt% for cores, 0.11–1.33 wt% for rims, see Tables 4 and 5). Magnetite cores contain 0.56–5.67% Al_2O_3 with an average of 2.78%. Spinel component in magnetite core varies between 1.16 and 14.47% with an average of 5.54% (Table 4). Al_2O_3 contents in magnetite rims range from 0.52 to 1.21% with an average of 0.86%, and spinel component ranges from 1.10 to 2.63% with an average of 1.81% (Table 5). The relatively high ulvöspinel and spinel components in magnetite core probably indicate high-temperature environment (see Deer et al., 1992).

The oxygen fugacity has a direct influence on the degree of solid solution between magnetite and ulvöspinel or between ilmenite and hematite. In Kokchetav 'lamproite', Ti–magnetite cores contain abundant exsolved ilmenite inclusions and equilibrium temperature and oxygen fugacities can be calculated. Two different magnetite–

Table 7
The representative compositions of biotite

Oxides, wt%	core	rim	core	rim	core	rim	core	rim	core	rim	core	rim	core	rim	core	rim	core	rim	core	rim
SiO_2	37.01	35.76	36.46	35.81	37.14	36.36	37.41	36.26	37.10	36.00	37.03	35.56	36.79	36.03	36.85	36.07	37.08	35.65	37.05	36.11
TiO_2	3.82	3.52	4.25	4.05	3.72	3.46	3.99	3.27	3.93	3.76	4.04	3.51	3.66	3.56	3.76	2.78	3.60	3.58	3.81	3.54
Al_2O_3	15.58	15.24	15.38	15.42	15.57	15.20	15.60	15.22	15.58	15.12	15.55	15.20	15.36	14.96	15.24	15.18	15.36	15.19	15.49	15.15
Cr_2O_3	0.05	0	0.04	0.11	0.06	0.01	0.01	0.10	0	0.04	0.04	0.04	0.08	0	0.09	0	0.02	0	0.02	0
BaO	0.55	0.55	0.61	0.69	0.50	0.47	0.56	0.53	0.49	0.55	0.61	0.47	0.51	0.50	0.58	0.50	0.56	0.49	0.60	0.51
CaO	0.01	0.35	0	0.34	0.03	0.25	0.05	0.10	0.01	0.04	0.02	0.05	0.02	0.02	0.06	0.33	0.04	0	0.04	0.09
FeO	12.59	20.66	12.57	19.73	12.48	18.07	12.26	18.26	12.50	19.62	11.77	19.74	12.77	16.71	12.49	20.66	11.85	19.41	11.95	20.01
MgO	17.30	10.77	17.00	11.41	17.72	13.11	17.04	12.24	17.51	11.87	17.19	11.60	17.33	12.89	17.18	11.50	17.49	11.61	17.34	12.03
Na_2O	0.20	0.08	0.19	0.06	0.14	0.14	0.16	0.09	0.20	0.10	0.17	0.13	0.13	0.14	0.14	0.07	0.22	0.14	0.16	0.11
K_2O	9.50	9.44	9.58	9.19	9.51	9.10	9.63	9.44	9.78	9.47	9.56	9.48	9.58	9.34	9.62	9.11	9.63	9.43	9.45	9.27
P_2O_5	0.02	0	0.05	0.01	0	0.02	0.01	0	0.05	0	0.03	0.01	0.02	0	0.03	0.03	0.01	0.04	0.10	0.01
Total	96.64	96.37	96.13	96.82	96.88	96.18	96.72	95.51	97.15	96.57	96.01	95.78	96.26	94.15	96.03	96.23	95.86	95.53	96.00	96.82
Cation (O=22)																				
Si	5.420	5.472	5.382	5.426	5.420	5.483	5.462	5.524	5.407	5.464	5.441	5.450	5.419	5.529	5.438	5.508	5.461	5.465	5.443	5.466
Ti	0.421	0.405	0.472	0.462	0.408	0.392	0.438	0.375	0.431	0.429	0.446	0.405	0.405	0.411	0.417	0.319	0.399	0.413	0.421	0.403
Al	2.689	2.749	2.676	2.754	2.678	2.702	2.685	2.733	2.676	2.705	2.693	2.746	2.667	2.706	2.651	2.732	2.666	2.745	2.682	2.703
Cr	0.006	0.000	0.005	0.013	0.007	0.001	0.001	0.012	0.000	0.005	0.005	0.005	0.009	0.000	0.011	0.000	0.003	0.000	0.003	0.000
Ba	0.031	0.033	0.035	0.041	0.029	0.028	0.032	0.032	0.028	0.033	0.035	0.028	0.030	0.030	0.033	0.030	0.032	0.029	0.034	0.030
Ca	0.002	0.057	0.000	0.055	0.005	0.040	0.008	0.017	0.002	0.007	0.003	0.008	0.003	0.003	0.010	0.054	0.006	0.000	0.006	0.014
Fe	1.542	2.644	1.552	2.500	1.523	2.279	1.497	2.327	1.524	2.491	1.446	2.530	1.573	2.145	1.541	2.638	1.460	2.489	1.468	2.533
Mg	3.777	2.457	3.741	2.577	3.855	2.947	3.709	2.780	3.804	2.686	3.765	2.650	3.805	2.949	3.779	2.618	3.840	2.653	3.798	2.715
Na	0.057	0.024	0.054	0.019	0.040	0.041	0.046	0.025	0.056	0.030	0.048	0.038	0.038	0.041	0.039	0.020	0.064	0.040	0.045	0.032
K	1.775	1.843	1.804	1.777	1.771	1.751	1.794	1.835	1.818	1.834	1.792	1.854	1.800	1.829	1.811	1.775	1.809	1.844	1.771	1.790
P	0.003	0.000	0.006	0.001	0.000	0.002	0.001	0.000	0.006	0.000	0.004	0.001	0.003	0.000	0.004	0.005	0.001	0.005	0.012	0.001
$Mg^{\#}$	71.0	48.2	70.7	50.8	71.7	56.4	71.2	54.4	71.4	51.9	72.2	51.2	70.8	57.9	71.0	49.8	72.5	51.6	72.1	51.7

Table 7 (*Continued*).
The representative compositions of biotite

Oxides, wt%	core	rim	core	rim	core	rim	core	rim	core	rim	core	rim	core	rim	core	rim	core
SiO_2	36.64	36.16	36.95	36.18	36.88	36.12	36.87	36.26	35.45	35.43	35.88	35.71	35.69	35.35	36.49	35.92	36.24
TiO_2	4.05	3.66	4.06	3.89	4.17	4.09	3.83	3.45	4.52	3.79	3.75	3.28	3.64	3.64	3.83	3.57	3.32
Al_2O_3	15.55	15.16	15.26	15.02	15.44	15.21	15.51	15.37	15.08	14.85	15.47	14.95	15.26	14.99	15.61	15.29	15.69
Cr_2O_3	0.05	0.05	0	0.02	0	0.10	0.12	0.05	0	0	0	0	0	0	0.02	0.02	0.05
BaO	0.61	0.49	0.51	0.45	0.54	0.58	0.60	0.46	1.27	1.37	0.65	1.78	1.35	0.73	0.89	0.92	1.01
CaO	0.07	0.09	0.03	0.09	0.05	0.41	0.01	0.04	0	0	0	0	0	0	0.06	0.10	0.02
FeO	11.53	18.87	11.80	17.99	11.77	19.94	12.41	18.58	15.97	18.91	12.01	19.67	15.81	18.69	11.81	16.55	12.75
MgO	17.35	11.74	17.14	12.61	17.37	11.09	17.60	12.49	13.49	11.23	16.95	11.15	14.15	11.28	16.71	13.35	16.81
Na_2O	0.21	0.10	0.23	0.12	0.21	0.09	0.17	0.12	0	0	0	0	0	0	0.18	0.11	0.04
K_2O	9.46	9.41	9.59	9.45	9.32	9.14	9.65	9.61	10.02	9.73	10.46	10.02	10.30	9.85	10.49	10.26	10.16
P_2O_5	0	0.02	0	0.01	0.01	0.05	0.01	0	0	0	0	0	0	0	0	0	0
Total	95.52	95.74	95.57	95.83	95.75	96.82	96.78	96.43	95.79	95.31	95.17	96.55	96.19	94.52	96.08	96.08	96.08
Cation (O= 22)																	
Si	5.411	5.510	5.456	5.486	5.427	5.469	5.398	5.480	5.389	5.485	5.371	5.496	5.407	5.489	5.409	5.445	5.390
Ti	0.450	0.419	0.451	0.444	0.462	0.466	0.422	0.392	0.517	0.441	0.422	0.380	0.414	0.425	0.427	0.407	0.371
Al	2.707	2.723	2.656	2.685	2.678	2.715	2.677	2.738	2.703	2.709	2.729	2.713	2.724	2.743	2.727	2.732	2.750
Cr	0.006	0.006	0.000	0.003	0.000	0.012	0.014	0.005	0.000	0.000	0.000	0.000	0.000	0.000	0.002	0.003	0.006
Ba	0.036	0.029	0.030	0.027	0.031	0.035	0.034	0.027	0.076	0.083	0.038	0.107	0.080	0.045	0.053	0.056	0.060
Ca	0.011	0.014	0.005	0.015	0.007	0.067	0.001	0.007	0.000	0.000	0.000	0.000	0.000	0.000	0.009	0.016	0.003
Fe	1.424	2.405	1.457	2.282	1.449	2.525	1.520	2.348	2.030	2.448	1.504	2.532	2.002	2.427	1.464	2.098	1.586
Mg	3.819	2.667	3.773	2.851	3.811	2.503	3.841	2.814	3.057	2.591	3.782	2.557	3.194	2.611	3.692	3.017	3.726
Na	0.059	0.029	0.066	0.036	0.059	0.025	0.050	0.036	0.000	0.000	0.000	0.000	0.000	0.000	0.053	0.033	0.013
K	1.782	1.829	1.807	1.828	1.750	1.766	1.803	1.853	1.943	1.922	1.997	1.967	1.991	1.951	1.984	1.983	1.928
P	0.000	0.002	0.000	0.001	0.001	0.006	0.001	0.000	0.000	0.000	0.000	0.000	0.000	0.000	0.000	0.000	0.000
$Mg^{\#}$	72.8	52.6	72.1	55.5	72.5	49.8	71.7	54.5	60.1	51.4	71.6	50.2	61.5	51.8	71.6	59.0	70.1

$Mg^{\#} = 100\ Mg/(Mg+Fe)$

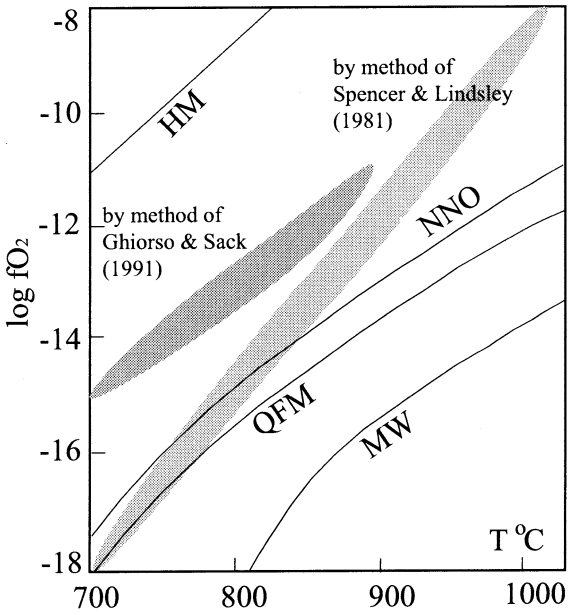

Fig. 9. Temperature–fO_2 plot showing the calculated temperature and oxygen fugacity of ilmenite-bearing magnetite based on the methods of Spencer and Lindsley (1981) and Ghiorso and Sack (1991), respectively. Curves define solid oxygen buffers corresponding to hematite–magnetite (HM; Myers and Eugster, 1983), quartz–fayalite–magnetite (QFM; Berman, 1988), and magnetite–wüstite (MW; Myers and Eugster, 1983).

ilmenite thermometry/oxygen barometers (Spencer and Lindsley, 1981; Ghiorso and Sack, 1991) were used to estimate the temperature and oxygen fugacity of Kokchetav 'lamproite' magma. Each produced different temperature and oxygen fugacity (Fig. 9). The calculated temperature by Spencer and Lindsley (1981) is highly variable (between 300 and 1143°C), and the log fO_2 varies between −9.6 and −19.2 at temperatures of 700–1100°C. The method of Ghiorso and Sack (1991) gives relatively reasonable temperature (679–887°C) and less variable log fO_2 values (between −11.1 and −14.9). All these values were derived for magnetite cores with abundant ilmenite inclusions. Because the ilmenite-bearing magnetite cores are inhomogeneous in composition (Fig. 8), the equilibration between the magnetite and ilmenite is perhaps incomplete. This is probably the cause for the scattering of the temperature in Fig. 9.

As there is no ilmenite exsolution in magnetite rims, and no ilmenite is found near magnetite rims, temperature and oxygen fugacity cannot be calculated for magnetite rims by either of these methods. The large differences in both composition and structure between the rims and cores suggest that the temperature for magnetite rims should be different from the cores; magnetite rims probably formed at relatively lower temperature. However, as ilmenite lamellae were probably formed by high-temperature oxidation, where original Ti–magnetite was oxidized and re-

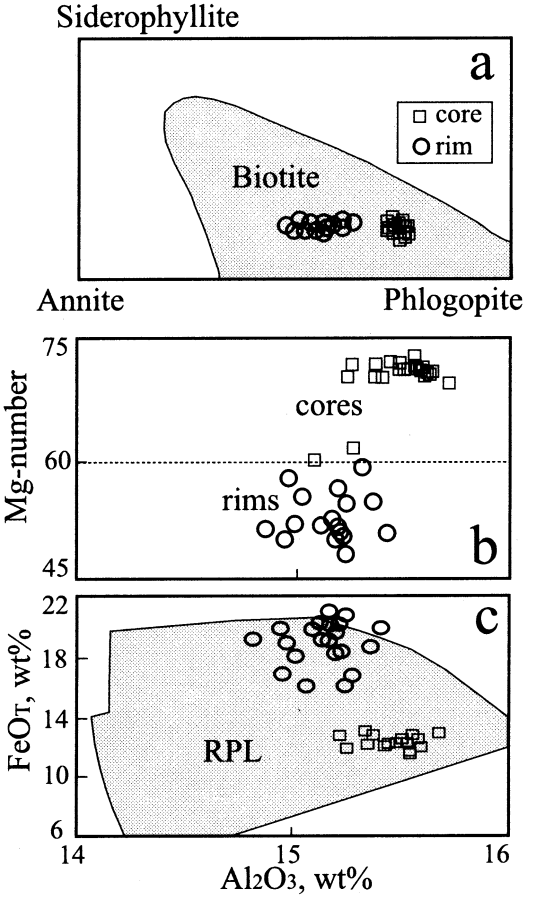

Fig. 10. Diagrams showing composition variations of biotite. (a) Biotite cores locate close to phlogopite end-member relative to biotite rims. Shaded area is the natural biotite composition space by Deer et al. (1992). (b) Mg-number versus Al_2O_3 plot, in which biotite cores differ from biotite rims by higher Mg-numbers. (c) Total FeO versus Al_2O_3 plot, where biotite rims differ from cores by higher FeO contents, shaded area is the RPL based on Mitchell and Bergman (1991).

Table 8
K-feldspar in groundmass of Kokchetav 'lamproite' (formula is calculated based on $O=8$)

Oxides, wt%	85	86	89	162	177	12	14	67	68	69	70	74	75	125	149	150	154	159
SiO_2	63.67	63.99	64.34	64.60	64.74	64.62	63.68	65.83	65.55	65.21	64.79	65.86	65.58	65.87	63.94	64.70	64.19	64.46
TiO_2	0	0.03	0.10	0.07	0	0.02	0	0	0	0.02	0	0	0.01	0	0.15	0.10	0.01	0.54
Al_2O_3	18.12	18.38	18.06	18.55	17.86	18.04	19.34	18.03	18.10	18.19	18.03	17.74	17.62	18.02	18.19	18.38	18.38	18.34
MgO	0.01	0.11	0	0.07	0.04	0	0	0	0	0	0	0	0	0	0	0	0.01	0
FeO	0.27	0.42	0.26	0.38	0.47	0.13	0.05	0.10	0.13	0.11	0.19	0.35	0.22	0.17	0.27	0.16	0.12	0.22
CaO	0.03	0.21	0.13	0.13	0.92	0.02	0.42	0	0.01	0	0.01	0.11	0.08	0.04	0.13	0.13	0.21	0.59
Na_2O	0.65	0.25	0.27	0.26	0.21	0.19	0.90	0.23	0.30	0.22	0.23	0.19	0.26	0.20	0.24	0.25	0.28	0.36
K_2O	15.97	15.67	15.91	16.00	15.84	16.00	14.56	16.27	16.44	16.80	16.28	16.14	16.44	16.36	16.18	16.41	16.33	16.00
Total	98.72	99.06	99.07	100.06	100.08	99.02	98.95	100.46	100.53	100.55	99.53	100.39	100.21	100.66	99.10	100.13	99.53	100.51
Cation ($O=8$)																		
Si	2.988	2.985	3.001	2.986	2.998	3.011	2.959	3.023	3.014	3.004	3.010	3.029	3.027	3.022	2.988	2.991	2.987	2.972
Ti	0	0.001	0.004	0.003	0	0.001	0	0	0	0.001	0	0	0	0	0.005	0.004	0.001	0.019
Al	1.002	1.011	0.993	1.010	0.974	0.991	1.059	0.976	0.981	0.988	0.987	0.961	0.958	0.974	1.002	1.002	1.008	0.996
Mg	0.001	0.007	0	0.005	0.003	0	0	0	0	0	0	0	0	0	0	0	0.001	0
Fe	0.011	0.016	0.010	0.015	0.018	0.005	0.002	0.004	0.005	0.004	0.007	0.014	0.008	0.007	0.011	0.006	0.005	0.009
Ca	0.002	0.010	0.007	0.006	0.045	0.001	0.021	0	0.001	0	0	0.006	0.004	0.002	0.007	0.006	0.011	0.029
Na	0.060	0.023	0.024	0.023	0.018	0.017	0.081	0.021	0.027	0.020	0.021	0.017	0.023	0.018	0.021	0.023	0.026	0.032
K	0.956	0.933	0.946	0.943	0.936	0.951	0.863	0.953	0.964	0.987	0.965	0.947	0.968	0.958	0.965	0.968	0.970	0.941
Mol%																		
Ab	5.85	2.34	2.480	2.37	1.84	1.79	8.40	2.10	2.70	1.94	2.09	1.72	2.317	1.81	2.15	2.27	2.55	3.19
An	0.14	1.08	0.67	0.64	4.55	0.08	2.16	0	0.06	0.00	0.04	0.57	0.38	0.21	0.67	0.63	1.05	2.89
Or	94.04	96.58	96.85	96.99	93.61	98.13	89.43	97.90	97.24	98.05	97.87	97.71	97.31	97.98	97.18	97.10	96.41	93.92

Table 9
Albite in groundmass of Kokchetav 'lamproite' (formula is calculated based on $O=8$)

Oxides, wt%	83	87	88	90	179	835	836	13	118	119	120	121	122	123	124
SiO_2	67.55	67.44	67.15	66.96	68.98	65.54	67.42	67.86	68.88	68.69	69.49	69.03	69.42	69.20	68.74
TiO_2	0.01	0	0	0	0.01	0.02	0	0	0	0.01	0	0	0	0.01	0.02
Al_2O_3	19.09	18.17	18.98	18.54	19.26	19.19	19.17	19.91	19.22	20.08	19.13	19.54	19.29	19.60	19.89
MgO	0.04	0.18	0.26	0.18	0.01	0.27	0.28	0	0.01	0	0	0	0	0	0
FeO	0.32	1.26	0.94	1.36	0.29	2.31	0.85	0.05	0.06	0	0	0.07	0	0.08	0.02
CaO	0.10	0.92	0.92	1.20	0.13	0.13	0.05	0.75	0.08	0.31	0.06	0.29	0.15	0.15	0.49
Na_2O	9.56	10.90	10.25	10.03	11.46	10.98	10.82	10.60	11.66	11.26	11.70	11.82	11.78	11.65	11.37
K_2O	3.02	0.24	0.89	1.19	0.11	0.58	0.73	0.59	0.07	0.20	0.06	0.14	0.10	0.10	0.21
Total	99.69	99.11	99.39	99.46	100.25	99.02	99.32	99.76	99.98	100.55	100.44	100.89	100.74	100.79	100.74
Cation ($O=8$)															
Si	2.994	2.997	2.976	2.978	3.006	2.937	2.982	2.976	3.007	2.982	3.017	2.993	3.009	2.998	2.983
Ti	0.001	0	0	0	0	0.001	0	0	0	0	0	0	0	0	0.001
Al	0.997	0.951	0.991	0.972	0.989	1.014	0.999	1.029	0.989	1.028	0.979	0.998	0.985	1.001	1.017
Mg	0.002	0.012	0.017	0.012	0.001	0.018	0.018	0	0.001	0	0	0	0	0	0
Fe	0.012	0.047	0.035	0.051	0.011	0.087	0.032	0.002	0.002	0	0	0.003	0	0.003	0.001
Ca	0.005	0.044	0.044	0.057	0.006	0.006	0.002	0.035	0.004	0.014	0.003	0.014	0.007	0.007	0.023
Na	0.822	0.939	0.880	0.865	0.968	0.954	0.928	0.901	0.987	0.948	0.985	0.994	0.990	0.979	0.957
K	0.171	0.013	0.050	0.068	0.006	0.033	0.041	0.033	0.004	0.011	0.003	0.008	0.005	0.006	0.012
Mol%															
Ab	82.40	94.27	90.35	87.39	98.74	96.08	95.52	92.95	99.21	97.40	99.38	97.92	98.78	98.71	96.53
An	0.50	4.38	4.49	5.77	0.61	0.60	0.23	3.63	0.38	1.46	0.29	1.33	0.69	0.72	2.30
Or	17.11	1.35	5.16	6.84	0.64	3.32	4.25	3.42	0.41	1.14	0.33	0.76	0.53	0.57	1.16

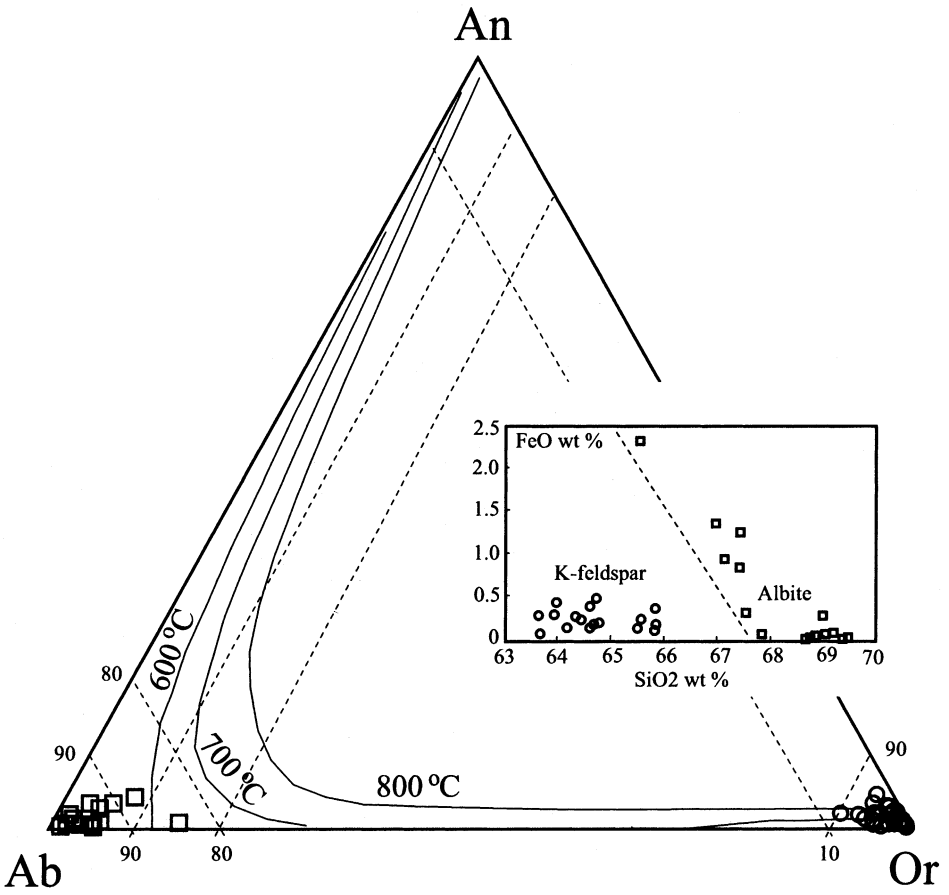

Fig. 11. The FeO versus SiO_2 plot and An–Ab–Or diagram showing the compositions of feldspar in the groundmass. Curves define the equilibrium temperature of the feldspars according to Kröll et al. (1993).

solved into secondary magnetite and ilmenite, the calculated temperatures for the ilmenite-bearing magnetite cores represent the condition for the high-temperature oxidation, which should happen at the same time when the ilmenite-free magnetite rim crystallized from magma. Therefore, above calculated temperatures should represent the crystallization temperature for the ilmenite-free magnetite rims. This implies that the ilmenite-bearing magnetite cores crystallized at even higher temperatures.

4.2.3. Biotite–phlogopite phenocryst

Biotite is a minor mineral phase in Kokchetav 'lamproite' (<1 vol.%), and occurs only as phenocryst (Fig. 2c). The representative biotite compositions are listed in Table 7 and shown in Fig. 10. Biotite is zoned with higher Mg contents in cores (phlogopite) than in rims (Fig. 10a). Mg-numbers are higher than 60 (four of them <70) for cores and lower than 60 for rims (Fig. 10b; Table 7). Phenocryst biotite throughout the studied rocks is essentially of similar composition, and the cores are Mg-rich relative to their rims. This observation suggests that the cores formed in Mg-rich magma, whereas rims crystallized in a differentiated magma. All the cores and most rims and characterized with high FeO and Al_2O_3 contents, which make the studied biotites similar to the phlogopite from the RPL (Fig. 10c).

4.2.4. Feldspar in matrix

The groundmass of Kokchetav 'lamproite' originally consists of micro-feldspar (~10 μm; albite and K-feldspar). The representative compositions of K-feldspar and albite are listed in Tables 8 and 9, respectively, and shown in Fig. 11. The An component ranges from 0 to 4.55 mol% in K-feldspar (Table 8), and from 0.23 to 5.77 mol% in albite (Table 9). FeO contents are significant in feldspar, especially in albite (0–2.31 wt%) relative to K-feldspar (0.05–0.80 wt%). High FeO content is considered to be a characteristic of feldspar crystallized from lamproitic magma (Mitchell and Bergman, 1991; Kuehner and Joswiak, 1996). The hydrothermal alteration mainly occurs in matrix; epidote and actinolite have replaced feldspar partially. Due to the hydrothermal process, feldspar can re-equilibrate at low temperature. Sanidine can decompose into two un-mix phases: albite and microcline (see temperature–composition diagram for Na–K-feldspar join at low pressure by Smith and Brown, 1988, p. 9). This probably suggests that original sanidine has been changed into albite and microcline at low pressure and temperature.

5. Discussion

The most peculiar character for the studied rocks is the significant difference of chemical composition between cores and rims of all phenocrysts (clinopyroxene, biotite–phlogopite and magnetite). The cores (Cr-rich diopside, phlogopite) seem to represent characters of lamproite, but the rims (Ti-rich salite, Fe-rich biotite) are highly different from lamproite. Another peculiar character of the studied rocks is the very high CaO and FeO contents in comparison with other potassic rocks, and abundant diopside phenocrysts occurring in this rocks cannot provide an explanation for the high CaO content due to low MgO contents in bulk composition. The distinct difference between core and rim, in addition to medium content of Al_2O_3 in bulk composition, suggests 'mixing' between two types of magma before eruption, however, FeO and CaO contents deny this hypothesis. Accordingly, the origin of the rock may be another interesting problem to be solved. We concentrate to the problems of magma differentiation and crystallization conditions here, and discuss the implications for the postcollisional magma evolution under the Kokchetav UHP terrain.

5.1. Magma differentiation and crystallization conditions

Cr is compatible and tends to partition into the early-crystallized mineral phases. The clinopyroxene core obviously served as the early-crystallized phase in lamproite magma, containing relatively more Cr_2O_3 than the rims. However, if magma evolved in a closed system, Cr content must decrease in residual magma due to clinopyroxene crystallization. Then, the late stage clinopyroxene should contain less Cr, even if crystallization continued at the same P–T conditions. Clinopyroxene crystals have similar zoning patterns with high Mg-numbers and Cr contents

Table 10
Summary of the evolution of the Kokchetav 'lamproite'

Stage I	Stage II	Stage III
< Crystallized phases >		
Clinopyroxene core (Cr-rich diopside)	Clinopyroxene rim (Ti-rich salite)	No clinopyroxene (broken and resorbed)
Biotite core (phlogopite)	Biotite rim	No biotite
No magnetite	Magnetite core	Magnetite rim with exsolution of the core forming ilmenite inclusion
No feldspar	No feldspar	Sanidine (groundmass)
< Location >		
Deep chamber (mantle)	Shallow chamber (crust)	During and after eruption

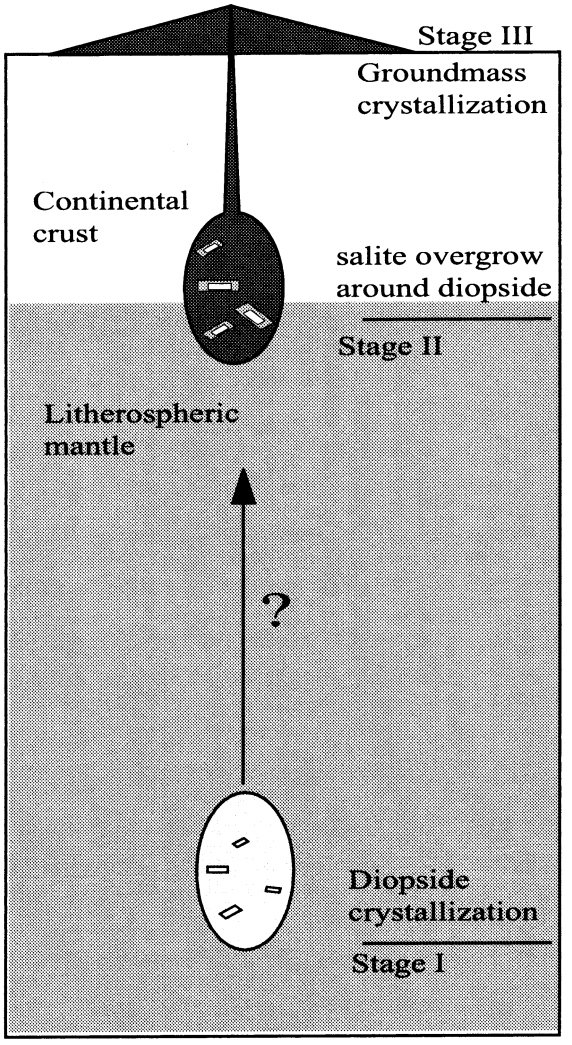

Fig. 12. Sketch showing three stages of magma evolution with two magma chambers (see text for detail).

(but lower Al^{VI} and Ti contents) in cores relative to rims. The apparent discontinuities in chemical composition of clinopyroxene phenocryst (Figs. 4–6) clearly demonstrate two stages of clinopyroxene crystallization. As mentioned before (4.2. Mineral compositions), one at HP corresponds to the cores, another at low pressure corresponding to the rims. However, magma differentiation can play an important role during each of these stages, and therefore produce highly variable Mg-numbers and Cr-numbers (Fig. 6).

Ti–magnetite crystallization probably happened at the time when magma was transferred from HP to lower pressure chamber, as there are abundant Ti–magnetite inclusions in clinopyroxene rims (Fig. 2b) and clinopyroxene cores are inclusion-free. This observation implies that the fO_2 values of magma greatly change from which clinopyroxene cores crystallized to which clinopyroxene rims and magnetite crystallized. The fO_2 values probably increased as magnetite crystallized in the shallow magma chamber at low pressure. The abundant ilmenite inclusions in magnetite core (see Fig. 3) suggest that Ti content in magma was high relative to the magma from which the magnetite rim crystallized. Such high-Ti magma probably corresponds to the magma from which clinopyroxene rims crystallized, as clinopyroxene rims are significantly enriched in Ti relative to their cores (see Figs. 5 and 6). Ti–magnetite cores and clinopyroxene rims probably crystallize in the same magma at the same time, because magnetite inclusions are abundant only in the clinopyroxene rim (see Fig. 2b). This process should happen in a shallow magma chamber. If the ilmenite–magnetite pairs are in equilibrium, the temperature is calculated to be from 679 to 887°C (see Fig. 9), and the log fO_2 is calculated to be from −11.1 to −14.9 log units based on the theromobarometric method of Ghiorso and Sack (1991). The magnetite rims probably formed during magma eruption at the same time when groundmass crystallized, as magnetite occurring in the matrix has the same composition as the magnetite phenocryst rim, which is ilmenite inclusion-free and contains lower TiO_2 than magnetite phenocryst cores. Ilmenite exsolution in magnetite probably occurred during magma eruption from shallow magma chamber to surface. In this case, the obtained temperature and fO_2 values represent the condition during the eruption.

5.2. Implications for magma evolution

At least three stages can be identified in Kokchetav magma evolution (Table 10; Fig. 12). Stage I is represented by clinopyroxene cores formed in a deep magma chamber, probably at mantle condition. At this stage, the magma should be Mg- and Cr-rich as shown by diopside

compositions (see Fig. 5). Mg-rich biotite cores (phlogopite) probably also crystallized at this stage.

Stage II is represented by clinopyroxene salite rims, which crystallized in a shallow magma chamber. Most clinopyroxene rims contain little Cr. The absence of clinopyroxene in groundmass and the observation that most clinopyroxene phenocrysts were broken and embayed by matrix (see Fig. 2) suggest clinopyroxene phenocryst stopped growing before magma eruption. The large difference between clinopyroxene cores and rims shown in Figs. 5 and 6 indicates that the environment of crystal growth greatly changed from deep magma chamber to shallow chamber. Fe-rich biotite rims and Ti–magnetite cores probably co-exist with clinopyroxene salite rims and formed in the shallow chamber at this stage.

Stage III of magma evolution is represented by matrix crystallization during and after magma eruption. The inclusion-free rims of magnetite phenocryst probably also crystallized at this stage. Only feldspar (probably sanidine) with small amounts of apatite and magnetite crystallized from the quenched magma at this stage. As K and Na contents in clinopyroxene are very low, and there is only very small amount of biotite (<1 vol.%) in Kokchetav 'lamproite', the major alkali phase is feldspar. Therefore, alkali elements mainly concentrated in matrix only at the latest stage of magma evolution.

6. Conclusions

The mineral characteristics in Kokchetav 'lamproite' suggest at least three phases of crystallization. Clinopyroxene cores (diopside) and Mg-rich biotite cores (phlogopite) crystallized at HP in a deep magma chamber. The magma and diopside were transferred to a shallow chamber where salite overgrew on diopside and Ti–magnetite crystallized, and the Fe-rich biotite rim overgrew on its Mg-rich phases. The magnetite rims probably formed during magma eruption at the same time when groundmass crystallized. The calculated temperatures for ilmenite–magnetite pair range from 679 to 887°C, log fO_2 values range from -11.1 to -14.9 log units. Ilmenite exsolution in magnetite occurred during magma eruption from shallow magma chamber to surface. Magma differentiation in the shallow magma chamber is completely developed before eruption, and produced alkali-rich residual magma.

Acknowledgements

We thank Mr. Yonemochi Kenji (Waseda Univ.) for his help to perform the electronic microprobe analysis and X-ray mapping. We are grateful to Dr. M.A. Kassymov (Institute of Geological Sciences, Kazakhstan) for his help in the field trip. Dr. Y. Kaneko, S. Maruyama (TIT) and others of the Japanese Kokchetav mapping team are appreciated for collection of abundant rock samples. Dr. John Richards (Oregon University) carefully reviewed the early version of this manuscript. His suggestions helped us to improve this work. Many thanks to Dr. Steven Bergman (Southern Methodist University) and an anonymous reviewer of Journal of Volcanology and Geothermal Research; their suggestions helped us to improve this manuscript greatly. The National Science Foundation of China (No. 40073025) and the exchange program between Peking University and Waseda University for Y.Z. supported this research.

References

Bergman, S.C., 1987. Lamproites and other potassium-rich igneous rocks: A review of their occurrence, mineralogy and geochemistry. In: Fitton and Upton, q.v., pp. 103–190.

Berman, P.G., 1988. Internally-consistent thermodynamic data for minerals in the system Na_2O-K_2O-CaO-MgO-FeO-Fe_2O_3-Al_2O_3-SiO_2-TiO_2-H_2O-CO_2. J. Petrol. 29, 445–522.

Brey, G.P., Nickel, K.G., Kogarko, L., 1986. Garnet-pyroxene equilibria in the system CaO-MgO-Al_2O_3-SiO_2 (CMAS): Prospects for simplified ('T-independent') lherzolite barometry and an eclogite-barometer. Contrib. Mineral. Petrol. 92, 448–455.

Claoue-Long, J.C., Sobolev, N.V., Shatsky, V.S., Sobolev, A.V., 1991. Zircon response to diamond-pressure metamorphism in the Kokchetav massif, USSR. Geology 19, 710–713.

Deer, W.A., Howie, R.A., Zussman, J., 1992. An Introduction to the Rock-Forming Minerals, 2nd edn. Longman, Harlow, 696 pp.

Dobretsov, N.L., Sobolev, N.V., Shatsky, V.S., Coleman, R.G., Ernst, W.G., 1995. Geotectonic evolution of diamondferious parageneses, Kokchetav Complex, northern Kazakhstan: The geologic enigma of ultrahigh-pressure crustal rocks within a Paleozoic fold belt. Isl. Arc 4, 267–279.

Ghiorso, M.S., Sack, R.O., 1991. Fe-Ti oxide geothermometry: Thermodynamic formulation and the estimation of intensive variables in silicate magmas. Contrib. Mineral. Petrol. 108, 485–510.

Jagoutz, E., Shatsky, V.S., Sobolev, N.V., 1990. Sr-Nd-Pb isotopic study of ultrahigh PT rocks from Kokchetav massif. EOS Trans. Am. Geophys. Union 71, 1707.

Kaneko, Y., Maruyama, S., Terabayashi, M., Yamamoto, H., Ishikawa, M., Anma, R., Parkinson, C.D., Ota, T., Nakajima, M., Katayama, I., Yamamoto, J., Yamauchi, K., 2000. Geology of the Kokchetav UHP-HP metamorphic belt, northern Kazakhstan. Isl. Arc 9, 264–283.

Kröll, H., Erangelakalis, C., Voll, G., 1993. Two-feldspar geothermometry: A review and revision for slowly cooled rocks. Contrib. Mineral. Petrol. 114, 510–518.

Kuehner, S.M., Joswiak, D.J., 1996. Naturally occurring ferric iron sanidine from the Leucite Hills lamproite. Am. Mineral. 81, 229–237.

Le Maitre, R.W., Bateman, P., Dudek, A., Keller, J., Lameyre, Le Bas, M.J., Sabine, P.A., Schmid, R., Sorensen, H., Streckeisen, A., Woolley, A.R., Zanettin, B., 1989. A Classification of Igneous Rocks and Glossary of Terms. Blackwell, Oxford.

Mitchell, R.H., 1995. Kimberlites, Orangeites, and Related Rocks. Plenum Press, New York, 410 pp.

Mitchell, R.H., Bergman, S.C., 1991. Petrology of Lamproites. Plenum Press, New York, 447 pp.

Morimoto, N., 1989. Nomenclature of pyroxenes. Can. Mineral. 27, 143–156.

Myers, J., Eugster, H.P., 1983. The system Fe-Si-O: Oxygen buffer calibrations to 1500 K. Contrib. Mineral. Petrol. 82, 75–90.

Nimis, P., Taylor, W.R., 2000. Single clinopyroxene thermobarometry for garnet peridotites. Part I. Calibration and testing of a Cr-in-Cpx barometer and an enstitite-in-Cpx thermometer. Contrib. Mineral. Petrol. 139, 541–554.

Ramsay, R.R., 1992. Geochemistry of Diamond Indicator Minerals. PhD Thesis. University of Western Australia, Perth, WA.

Shatsky, V.S., Jagoutz, E., Sobolev, N.V., Kozmenko, O.A., Parkhomenko, V.S., Troesch, M., 1999. Geochemistry and age of ultrahigh pressure metamorphic rocks from the Kokchetav massif (Northern Kazakhstan). Contrib. Mineral. Petrol. 137, 185–205.

Smith, J.V., Brown, W.L., 1988. Feldspar Minerals, 1. Crystal Structures, Physical Chemical and Microtextural Properties. Springer, Berlin, 828 pp.

Spencer, K.J., Lindsley, D.H., 1981. A solution model for coexisting iron-titanium oxides. Am. Mineral. 66, 1189–1201.

Thompson, R.N., 1974. Some high-pressure pyroxenes. Mineral. Mag. 39, 768–787.

Wass, S.Y., 1979. Multiple origins of clinopyroxenes in alkali basaltic rocks. Lithos 12, 115–132.